

# OPTICAL SPECTROSCOPY OF THE *IRAS* 1-Jy SAMPLE OF ULTRALUMINOUS INFRARED GALAXIES

Sylvain Veilleux<sup>1,2</sup>, D.-C. Kim<sup>2,3</sup> and D. B. Sanders<sup>4</sup>

## ABSTRACT

This paper discusses the optical spectroscopic properties of the *IRAS* 1-Jy sample ( $f_{60} > 1$  Jy) of ultraluminous infrared galaxies (ULIGs:  $L_{\text{ir}} > 10^{12} L_{\odot}$ ;  $H_0 = 75 \text{ km s}^{-1} \text{ Mpc}^{-1}$  and  $q_0 = 0$ ). One hundred and eight of the 118 1-Jy ULIGs have been observed at  $\Delta\lambda = 8.3 \text{ \AA}$  resolution over the wavelength range  $\sim 4500 \text{ \AA} - 8900 \text{ \AA}$ . These data are combined with large, previously published sets of optical spectroscopic data of lower luminosity infrared galaxies to look for systematic trends with infrared luminosity over the luminosity range  $L_{\text{ir}} \approx 10^{10.5} - 10^{13} L_{\odot}$ . As found in previous studies, the fraction of Seyfert galaxies among luminous infrared galaxies increases abruptly above  $L_{\text{ir}} \approx 10^{12.3} L_{\odot}$  — about 50% of the galaxies with  $L_{\text{ir}} > 10^{12.3} L_{\odot}$  present Seyfert characteristics. Many of the optical and infrared spectroscopic properties of the Seyfert galaxies are consistent with the presence of a genuine active galactic nucleus (AGN). About 30% of these galaxies are Seyfert 1s with broad-line regions similar to those of optical quasars. Published near-infrared spectroscopy also suggests that many of the Seyfert 2 galaxies (especially those with warm *IRAS* 25-to-60  $\mu\text{m}$  colors) are in fact obscured Seyfert 1 galaxies with broad ( $\gtrsim 2,000 \text{ km s}^{-1}$ ) recombination lines at  $2 \mu\text{m}$ , where dust obscuration is less important. The percentage of Seyfert 1 ULIGs increases with infrared luminosity, contrary to the predictions of the standard unification model for Seyfert galaxies. Comparisons of the broad-line luminosities of optical and obscured Seyfert 1 ULIGs with those of optically selected quasars of comparable bolometric luminosity suggest that the dominant energy source in most of these ULIGs is the same as in optical quasars, namely mass accretion onto a supermassive black hole, rather than a starburst. These results are consistent with recently published *ISO*, *ASCA*, and VLBI data.

On the other hand, there is no unambiguous optical or near-infrared spectroscopic evidence for an AGN in ULIGs optically classified as H II-region galaxies ( $\sim 30\%$  of the

---

<sup>1</sup>Department of Astronomy, University of Maryland, College Park, MD 20742; E-mail: veilleux@astro.umd.edu

<sup>2</sup>Visiting observers at the Kitt Peak National Observatory of the National Optical Astronomy Observatories, operated by AURA, Inc., for the National Science Foundation.

<sup>3</sup>Infrared Processing and Analysis Center, California Institute of Technology, Pasadena, CA 91125; E-mail: kim@ipac.caltech.edu

<sup>4</sup>Institute for Astronomy, University of Hawaii, 2680 Woodlawn Drive, Honolulu, HI 96822; E-mail: sanders@ifa.hawaii.edu

whole sample) or as LINERs ( $\sim 40\%$ ). The apparent lack of an energetically important AGN in these objects supports the results from recent mid-infrared spectroscopy with ISO. Photoionization by hot stars from a recent starburst appears to be the dominant source of ionization in the objects with HII region-like spectra, while both hot stars and shocks may contribute to the ionization in ULIGs with LINER-like spectra. The weaker  $H\beta$  and Mg Ib stellar absorption features, larger  $H\alpha$  emission equivalent widths and bluer optical continuum colors in objects of higher infrared luminosities suggests that the starburst took place more recently ( $\lesssim \text{few} \times 10^7$  yrs) and/or is more important ( $\sim 10\%$  of the galaxy mass) in ULIGs than in their lower luminosity counterparts.

As found in optically-selected starbursts, the emission-line gas in ULIGs is dustier than the stellar population which is producing the optical continuum. The color excess derived from the Balmer line ratio does not significantly depend on the infrared luminosity, optical spectral type, or *IRAS* 25-to-60  $\mu\text{m}$  color of the luminous infrared galaxies. These results suggest that the optical method used to determine the color excess in infrared galaxies underestimates the amount of dust in the dustier objects.

*Subject headings:* galaxies: nuclei — galaxies: stellar content galaxies : Seyfert — infrared: sources

## 1. Introduction

The nature of the dominant energy source in ultraluminous infrared galaxies (ULIGs:  $L_{\text{ir}} > 10^{12} L_{\odot}$ )<sup>5</sup> is the object of a vigorous debate (see, e.g., review by Sanders & Mirabel 1996). Results from recent studies at mid-infrared (e.g., Lutz et al. 1996, 1998; Genzel et al. 1998) and radio wavelengths (Lonsdale et al. 1998; Smith et al. 1998a,b) suggest that several ULIGs are powered predominantly by hot stars rather than by an active galactic nucleus (AGN). However, the great majority of the infrared galaxies in these samples are of relatively modest luminosity, with only a few having  $L_{\text{ir}} > 2 \times 10^{12} L_{\odot}$ . This distinction may be important as there is growing evidence from optical/near-infrared spectroscopy that the frequency of occurrence of AGN among luminous infrared galaxies (LIGs:  $L_{\text{ir}} \gtrsim 10^{11} L_{\odot}$ ) increases with increasing infrared luminosity. Veilleux et al. (1995; hereafter VKSMS) carried out a sensitive optical spectroscopic survey of a sample of 200 LIGs and classified the nuclear spectra of these galaxies using a large number of optical line-ratio diagnostics corrected for the underlying stellar absorption features. VKSMS found that 7 of the 21 ULIGs in their sample showed Seyfert characteristics. In contrast, only 19 of the 161 objects with lower luminosities ( $L_{\text{ir}} < 10^{12} L_{\odot}$ ) were optically classified as Seyferts. More recently, Kim, Veilleux, & Sanders (1998; hereafter KVS) extended this type of analysis to a subset of 45 ULIGs from the *IRAS* 1-Jy sample (Kim 1995; Kim & Sanders 1998). The fraction of Seyfert 1 and 2 galaxies among LIGs was found to increase dramatically above  $L_{\text{ir}} \approx 10^{12.3} L_{\odot}$  with more than 50% of the galaxies with  $L_{\text{ir}} > 10^{12.3} L_{\odot}$  having Seyfert characteristics. Near-infrared spectroscopy of a representative subset of ULIGs from the 1-Jy sample appears to confirm the presence of an energetically important AGN in many of these Seyfert galaxies (Veilleux, Sanders, & Kim 1997, 1999b; hereafter VSK97 and VSK99, respectively).

It is clearly important to verify the results of KVS using the entire 1-Jy sample. This sample provides a complete list of the brightest ULIGs with  $F[60 \mu\text{m}] > 1 \text{ Jy}$  which is not biased toward ‘warm’ quasar-like objects. The ‘1-Jy’ sample contains 118 objects with  $z = 0.02 - 0.27$  and  $\log [L_{\text{ir}}/L_{\odot}] = 12.00 - 12.90$ . The infrared luminosities of these objects therefore truly overlap with the bolometric luminosities of optical quasars. The present paper discusses the optical spectra of 63 of the 73 ULIGs from the 1-Jy sample that were not observed by KVS, and combine these results with our previously published optical and near-infrared data to look for systematic trends with infrared luminosity among galaxies with  $L_{\text{ir}} \approx 10^{10.5} - 10^{13} L_{\odot}$ .

The structure of this paper is as follows. Section 2 discusses the procedures used to obtain and reduce the new data. The results derived from these data are described and compared with those of previous optical spectroscopic studies in §3. In §4, the implications of our results on the nature of the dominant energy source in these objects are discussed in the context of recent investigations at longer and shorter wavelengths. The main conclusions are summarized in §5. We use  $H_0 = 75 \text{ km s}^{-1} \text{ Mpc}^{-1}$  and  $q_0 = 0$  throughout this paper.

---

<sup>5</sup> $L_{\text{ir}} \equiv L(8 - 1000 \mu\text{m})$ , computed from the observed infrared fluxes in all four *IRAS* bands according to the prescription outlined in Perault (1987)

## 2. Observations and Data Reduction

The new spectroscopic data were obtained with the Gold Cam Spectrograph on the Kitt Peak 2.1-meter telescope. Table 1 lists the dates of the observations, grating used, spectral coverage, resolution, and seeing during the observations. The exposure times range from 300 sec to 3,600 sec depending on the  $R$  magnitude of each object (cf. Kim 1995). In all cases, a slit with a width of  $2''$  was used and the slit was positioned in the N-S direction ( $PA = 0^\circ$ ). Most of the observations were made under photometric conditions. Those that were not are indicated with a dagger ( $\dagger$ ) in Tables 3 – 5. The moderate seeing prevented us from extracting useful spatial information along the spectrograph slit. The results derived from the KPNO data therefore only refer to the nuclear regions. For consistency with VKSMS and KVS, the KPNO data were reduced using the same techniques as those used in these earlier papers. Once again, aperture-related effects were minimized using a window for the extraction of the nuclear spectrum that varied according to the redshift of each object so that it corresponds to a constant linear scale (total diameter) of 4 kpc for most of the galaxies, with the exceptions of three distant galaxies with  $z > 0.2$  (F00397–1312, F12032+1707, and F23499+2423)<sup>6</sup> for which an 8-kpc window was used. The spectra of the flux standard stars were used to remove the absorption bands near 6870 Å and 7620 Å produced by atmospheric O<sub>2</sub> (the B- and A-bands, respectively).

## 3. Results

The final calibrated spectra obtained at KPNO are plotted in Figure 1. Only 10 of the 118 sources in the 1-Jy sample could not be observed with the KPNO 2.1-meter telescope because of low declination and/or lack of time. Refer to Figure 1 in KVS to view the calibrated spectra of the 45 objects observed using the Mauna Kea facilities. Tables 2, 3 and 4 summarize the results of our analysis on the new KPNO data and combine them with those of KVS and VKSMS. The methods used to derive the various quantities listed in these tables are described in detail in Kim et al. (1995) and KVS and are summarized below.

The line fluxes were measured using two methods. First, the standard plotting package in IRAF (“splot”) was used to measure the flux of isolated emission lines. To deal with blended lines (e.g.,  $H\alpha + [N\ II] \lambda\lambda 6548, 6583$  and  $[S\ II] \lambda\lambda 6716, 6731$ ) and emission lines affected by stellar absorption features ( $H\beta$  and  $H\alpha$ ), we used “specfit”, an interactive IRAF procedure kindly provided by Gerard A. Kriss. This routine can fit a wide variety of emission-line, absorption-line, and continuum models to the observed spectrum. The input parameters for the fit were determined through “splot” in IRAF. We chose to fit the continuum with a simple first-order polynomial, and the emission and absorption lines with Gaussian profiles. The actual fitting was done via a

---

<sup>6</sup>Object names that begin with ‘F’ are sources identified in the *IRAS* Faint Source Catalog, Version 2 (FSC: Moshir et al. 1992)

chi-square minimization using a simplex algorithm. The output parameters were the flux levels and slopes of the underlying continuum emission, the fluxes, centroids, and widths (FWHM) of the emission lines, and equivalent widths, centroids, and widths (FWHM) of the absorption lines.

Uncertainties in the  $H\alpha$  fluxes are typically 25 – 50%. The other emission line fluxes listed in Table 3 are normalized to the observed  $H\alpha$  flux. The uncertainty in these relative flux ratios is typically 5 – 10%. Colons (:) and double colons (::) indicate values with relative uncertainties of about 25% and 50%, respectively. The adopted  $H\beta$  flux, listed in column (5), is the weighted average of the values obtained from the “splot” and “specfit” methods, with weights estimated from the relative uncertainties in the two types of measurements.

The absorption line strengths, line widths, and continuum measurements are presented in Table 4. Column (2) of Table 4 lists the equivalent widths of  $H\beta$  derived from the fitting method. These measurements are rather uncertain ( $\sim 50\%$ ) because of the generally strong  $H\beta$  emission line affecting the profile of this feature. Columns (3) and (4) list the equivalent widths of the Mg Ib  $\lambda 5174$  and Na ID  $\lambda 5896$  absorption lines, respectively. Note that the Na ID feature is blended with the emission line of He I at  $\lambda 5876$  in some galaxies. Column (5) of Table 4 lists the values of the line widths (FWHM) of [O III]  $\lambda 5007$ . This line was selected for line width measurements because it is strong in most ULIGs and free of any nearby emission or absorption lines (in contrast to  $H\alpha$ ). The line widths listed in Table 4 have been corrected for the finite instrument resolution of the data ( $\sim 8.3\text{\AA}$ ) using the quadrature method. This method assumes that the intrinsic and instrument profiles are Gaussian and gives corrected widths that are too large for profiles which are more peaky than Gaussians (e.g., the emission-line profiles in optically-selected AGN – Whittle 1985; Veilleux 1991). For this reason, the [O III]  $\lambda 5007$  line widths should be treated with caution. Uncertainties on these measurements are about  $\pm 100 - 200 \text{ km s}^{-1}$  or more. Corrected line widths below  $100 \text{ km s}^{-1}$  are flagged with a colon in Table 4 to emphasize the large uncertainties on these measurements. Finally, the intensity levels of the continuum near  $H\beta$  and  $H\alpha$  are listed in columns (6) and (7) as C4861 and C6563, respectively.

### 3.1. Spectral Classification

The results from the spectral analysis of the *IRAS* 1-Jy sample are quantitatively similar to those derived by KVS on the subsample of 45 objects. The emission-line ratio measurements used for this analysis are listed in Table 5 and are plotted in Figure 2. As described in the previous section, these line ratios were corrected for the underlying Balmer absorption features. For consistency with KVS and VKSMS, the same dereddening and spectral classification techniques were used in the analysis. The line ratios were corrected for reddening using the values of  $E(B-V)$  determined from the  $H\alpha/H\beta$  ratio and the Whitford reddening curve as parameterized by Miller & Mathews (1972; see next section). The boundaries of Veilleux & Osterbrock (1987) were used to classify each object as H II or AGN-like galaxies. These boundaries are based on large data sets on optically selected galaxies and the predictions of photoionization models by power-law

spectra and by hot stars. A distinction was made among AGN-like galaxies between the objects of high ( $[\text{O III}] \lambda 5007/\text{H}\beta \geq 3$ ) and low ( $[\text{O III}] \lambda 5007/\text{H}\beta \leq 3$ ) excitation. The first group represents the “classic” Seyfert 2 galaxies while galaxies in the second group were classified as LINERs (“low-ionization nuclear emitting regions”). This LINER definition differs from the original definition of Heckman (1980) which partly relies on the strength of the  $[\text{O II}] \lambda 3727$  line (this line is outside the wavelength range of our spectra). However, results from spectroscopic studies of optically selected objects (e.g., Veilleux & Osterbrock 1987) suggest that the two ways of defining LINERs are often (close to 95 % of the time) equivalent. Finally, galaxies with Fe II multiplets at  $\lambda\lambda 5100\text{--}5560$  and very broad ( $\Delta V_{\text{FWHM}} \gtrsim 2,000 \text{ km s}^{-1}$ ) H I Balmer and He I  $\lambda 5876$  emission lines were classified as Seyfert 1s.

Following VKSMS and KVS, ULIGs with double nuclei were assigned the more Seyfert-like spectral type of the two nuclei: galaxy pairs with spectral types H II – LINER, H II – Seyfert 2, H II – Seyfert 1, LINER – Seyfert 2, LINER – Seyfert 1, and Seyfert 1 – Seyfert 2 were classified as LINER, Seyfert 2, Seyfert 1, Seyfert 2, Seyfert 1, and Seyfert 1, respectively. These widely separated interacting systems are more common at lower luminosities (VKSMS; Kim 1995; Surace 1998; Veilleux, Kim, & Sanders 1999a). Consequently, this classification method of the double-nucleus systems is conservative in the sense that it overestimates the fraction of AGN among the lower luminosity objects and thus cannot explain the trends with infrared luminosity discussed below.

Out of the 108 ULIGs that make up our spectroscopic sample, 30 % (32/108) were found to have spectra characteristic of photoionization by hot stars (H II region-like). AGN-like emission lines were observed in 70 % (76/108) of the total sample including 9 % (10/108) Seyfert 1s, 21 % (23/108) Seyfert 2s, and 40 % (43/108) LINER-like objects. These results were combined with the measurements obtained by VKSMS for the LIGs from the Bright Galaxy Survey (BGS; Soifer et al. 1987, 1989) to search for systematic variations of the spectral types with infrared luminosity. For this exercise, ULIGs were further divided into two luminosity bins:  $10^{12} L_{\odot} \leq L_{\text{ir}} < 10^{12.3} L_{\odot}$  and  $L_{\text{ir}} \geq 10^{12.3} L_{\odot}$ . A summary of this analysis is given in Table 6 and plotted in Figure 3.

This figure confirms the tendency noted by VKSMS and KVS for the more luminous objects to be more Seyfert-like. As noted by KVS, only one Seyfert 1 (NGC 7469) has  $L_{\text{ir}} < 10^{12} L_{\odot}$ , whereas 48 % (15/31) of the galaxies with  $L_{\text{ir}} \geq 10^{12.3} L_{\odot}$  present Seyfert characteristics. The percentage of Seyfert 1s relative to Seyfert 2s increases with infrared luminosity (from  $\sim 0\%$  among LIGs up to  $\sim 50\%$  among ULIGs with  $L_{\text{ir}} > 10^{12.3} L_{\odot}$ ). This result is not compatible with the predictions of the standard unification model of Seyfert galaxies which purports that Seyfert 1s and 2s are basically the same kind of objects observed from different angles. The far-infrared emission in these objects is believed to be emitted more or less isotropically and therefore does not depend on viewing angle (e.g., Mulchaey et al. 1994). The trend with infrared luminosity in our data can be explained if the covering factor of the obscuring material (opening angle of torus?) in Seyfert ULIGs decreases with increasing infrared luminosity.

LINER-like galaxies constitute a large fraction (30–40 %) of the total sample regardless of  $L_{\text{ir}}$ . The LIGs classified as H II galaxies generally have low-excitation lines ( $[\text{O III}] \lambda 5007/\text{H}\beta < 3$ ; Fig. 2) and no detectable Wolf-Rayet emission features (e.g., combinations of He II  $\lambda 4686$ , He I  $\lambda 5876$ , C III  $\lambda 5696$ , N IV  $\lambda 5737$ , N III  $\lambda\lambda 4634, 4640$ , and 4642), confirming previous results (KVS; VKSMS; Leech et al. 1989; Armus et al. 1989; Allen et al. 1991; Ashby, Houck, & Hacking 1992; Ashby et al. 1995) and strongly arguing *against* a very recent burst ( $\ll 10^7$  yr) of star formation in these objects (cf. §3.5; Evans & Dopita 1985; McCall, Rybski, & Shields 1985; Allen et al. 1991). Therefore, there is no evidence at optical wavelengths for the type of extremely young ( $5 \times 10^6$  yrs) starbursts purported by Downes & Solomon (1998) to exist in Arp 220 and other ULIGs. The implications of this spectral classification are discussed in §4.

### 3.2. Reddening

Following KVS, the reddening in our sample galaxies was estimated using the emission-line  $\text{H}\alpha/\text{H}\beta$  ratios corrected for the underlying stellar absorption features. An intrinsic  $\text{H}\alpha/\text{H}\beta$  ratio of 2.85 was adopted for H II region-like galaxies (Case B Balmer recombination decrement for  $T = 10^4$  K and  $N_e = 10^4 \text{ cm}^{-3}$ ) and 3.10 for Seyferts and LINERs (e.g., Halpern & Steiner 1983 and Gaskell & Ferland 1984). For consistency with the studies of VKSMS and KVS, the Whitford reddening curve as parameterized by Miller & Mathews (1972) was used. The reddenings derived from this method are listed as color excesses,  $E(B-V)$ , in the third column of Table 5. Since all the objects in the 1-Jy sample lie at  $|b| > 30^\circ$ , no correction was made for Galactic reddening. Note that this method assumes that the obscuration is due to a foreground screen of dust and underestimates by a factor  $[\exp(\tau)-1]/\tau$  the actual amount of extinction if the line-emitting gas and dust are spatially mixed. Moreover, the adopted procedure does not take into account possible differences between Galactic and extragalactic reddening curves (e.g., Calzetti, Kinney, & Storchi-Bergmann 1994). However, these differences will be small at optical wavelengths.

The distribution of  $E(B-V)$  for the ULIGs of our sample is shown in Figure 4. The results are quantitatively similar to those of KVS. Not surprisingly, the color excesses measured in the ULIGs of our sample are considerably larger than those measured in optically-selected Seyfert and starburst galaxies (Dahari & De Robertis 1988) and in extragalactic H II regions (Kennicutt, Keel, & Blaha 1989). These results confirm the importance of dust in infrared-selected galaxies. The median  $E(B-V)$  are 0.80, 1.11 and 1.21 for the H II galaxies (30 objects), LINERs (45) and Seyfert 2 galaxies (22), respectively. Kolmogorov-Smirnov (K-S) tests indicate that the differences between the various spectral types are not significant. These color excesses are similar to those obtained by VKSMS in the lower-luminosity galaxies of the BGS [ $E(B-V) = 1.05, 1.24$ , and 1.07 for H II galaxies, LINERs, and Seyfert 2 galaxies, respectively]. However, VKSMS found that the color excesses of the LINERs were significantly larger than those of the H II and Seyfert 2 galaxies; this difference is not observed among the 1-Jy ULIGs.

The correlation reported by VKSMS between  $E(B-V)$  and the equivalent width of the Na ID

absorption feature,  $EW(\text{NaID})$ , in H II galaxies is also present, but at a weaker level, among our high-luminosity objects. The probability,  $P[\text{null}]$ , that this correlation is fortuitous is 0.04, 0.01, and 0.001 among the H II galaxies, LINERs, and Seyfert 2 galaxies of the 1-Jy sample. An important fraction of the NaID feature is therefore of interstellar origin. A similar correlation is observed between  $E(B-V)$  and the observed continuum colors of H II galaxies ( $P[\text{null}] = 3 \times 10^{-5}$ ) and LINERs ( $P[\text{null}] = 1 \times 10^{-4}$ ), but not among Seyfert 2 galaxies ( $P[\text{null}] = 0.16$ ). As first reported by VKSMS, these results suggest that the scatter in the continuum colors of the Seyfert LIGs is predominantly intrinsic rather than caused by variations in the amount of reddening from one object to the other (cf. §3.5 for a more detailed discussion of continuum colors).

The *IRAS* flux density ratio  $f_{25}/f_{60}$  is a well-known indicator of Seyfert activity in infrared galaxies (e.g., deGrijs et al 1985; Miley, Neugebauer & Soifer 1985). Galaxies with “warm” *IRAS* 25-to-60  $\mu\text{m}$  colors are generally believed to be less affected by dust obscuration than the “cooler” objects (e.g., Sanders et al 1988a,b; Surace et al. 1998; VSK97, VSK99). One should therefore expect to see a positive correlation between the *IRAS* 25-to-60  $\mu\text{m}$  color and the color excess in our sample; however, none is detected (Fig. 5). This result suggests that the color excess derived from the optical emission lines is not always a good indicator of the total column of material towards the nucleus of these objects. This problem is more severe in the cooler, dustier objects because the optical method saturates beyond  $\tau_V \sim 5$  or, equivalently,  $E(B-V) \sim 2$ . Extinction measurements at longer wavelengths are more reliable (e.g., VSK97, VSK99, Genzel et al. 1998).

### 3.3. Line Widths

Figure 6 shows the distribution of the [O III] line widths for each spectral type. The median line widths of the H II galaxies and LINERs are comparable ( $200 \text{ km s}^{-1}$  and  $320 \text{ km s}^{-1}$ ) whereas the [O III] line widths of Seyfert 1 and 2 galaxies are larger ( $1,120$  and  $610 \text{ km s}^{-1}$ , respectively). K-S tests confirm these differences. The probability that the line widths of H II galaxies and LINERs are drawn from the same population is 0.70, but it is less than 0.001 when comparing the line widths of H II and Seyfert galaxies, or when comparing the LINERs and Seyfert galaxies.

Figure 7 presents the distribution of [O III] line widths of the combined sample as a function of infrared luminosity and as a function of the *IRAS* flux density ratio  $f_{25}/f_{60}$ . The new data strengthen the conclusions of VKSMS and KVS: there is no obvious correlation between line width and infrared luminosity or *IRAS* color, but nearly all of the objects with line widths larger than  $600 \text{ km s}^{-1}$  have  $L_{\text{ir}} \gtrsim 10^{11} L_{\odot}$  (the only exception is the H II galaxy NGC 3597 which has  $\log [L_{\text{ir}}/L_{\odot}] = 10.91$ ). Objects with the most extreme profiles ( $\Delta V_{\text{FWHM}} \gtrsim 1200 \text{ km s}^{-1}$ ) all have  $L_{\text{ir}} \gtrsim 10^{12} L_{\odot}$ , optical Seyfert characteristics, and warm *IRAS* colors ( $f_{25}/f_{60} \gtrsim 0.12$ ). These results suggest that the nuclear activity in the more powerful Seyfert ULIGs contributes to the line broadening. Non-gravitational processes associated with AGN-driven outflows have been proposed by VKSMS and KVS to explain the broad and complex line profiles in the nuclear and circumnuclear regions of some LIGs.



### 3.4. Stellar Absorption Features

In Figures 8 and 9, the distributions of the equivalent widths of  $H\beta$  and Mg Ib are presented as a function of spectral type. These distributions are similar to those obtained by KVS in their subset of the 1-Jy sample. The conclusions derived by KVS on the stellar absorption features are therefore generally confirmed by the analysis of the entire 1-Jy sample. The median  $EW(H\beta)$  for the 1-Jy ULIGs (including those with undetected  $H\beta$ ) are 0.8 Å, 0.6 Å, 0.0 Å and 0.0 Å for the H II galaxies (30 objects), LINERs (43), Seyfert 2 galaxies (22), and Seyfert 1 galaxies (9), respectively. K-S tests indicate that the equivalent widths of Seyfert 1 and 2 galaxies are significantly smaller than those of LINERs and H II galaxies ( $P[\text{null}] \lesssim 0.01$ ). The equivalent widths of the 1-Jy ULIGs taken as a whole are also significantly smaller than those measured by VKSMS in the BGS LIGs ( $P[\text{null}] = 4 \times 10^{-9}$  when comparing both samples, and  $P[\text{null}] = 0.002$  and  $0.01$  for LINERs and H II galaxies, respectively. There are too few Seyfert galaxies among the BGS LIGs to carry out this analysis). The intermediate-age ( $10^8$ – $10^9$  yr) population of stars that is responsible for the  $H\beta$  absorption feature is therefore less prominent in our sample of ULIGs, possibly because the  $H\beta$  feature is diluted by a hot, featureless continuum from young stars (particularly in H II galaxies) or from an AGN (in the Seyfert galaxies).

The strength of the Mg Ib absorption feature provides additional constraints on the underlying stellar population in ULIGs. As found by KVS, the  $EW(\text{Mg Ib})$  for our sample of ULIGs [median values of 0.0 Å, 0.1 Å, 0.2 Å, and 0.0 Å for H II galaxies (30 objects), LINERs (43), Seyfert 2 galaxies (22), and Seyfert 1 galaxies (9), respectively] are considerably smaller than those measured in non-active spiral galaxies [ $EW(\text{Mg Ib}) = 3.5$ – $5.0$  Å: Keel 1983; Stauffer 1982; Heckman, Balick, & Crane 1980]. Moreover, *contrary* to KVS findings, the  $EW(\text{Mg Ib})$  for our sample of ULIGs are also significantly smaller than those measured in the BGS objects of VKSMS (1.12 Å, 1.49 Å, and 1.17 Å for H II galaxies, LINERs, and Seyfert 2 galaxies, respectively). The very weak  $H\beta$  and Mg Ib features in 1-Jy ULIGs can be explained if the age of the *dominant* stellar population in these objects is less than a few  $\times 10^7$  yrs and  $\sim 10\%$  of the galaxy mass is taking part in a burst of star formation (Bica, Alloin, & Schmidt 1990). Alternatively, an AGN may account for  $\sim 50$  –  $75\%$  of the optical continuum in some ULIGs (e.g., Seyfert 1 and 2 galaxies) and weaken the spectral signatures of the underlying old stellar population. The analysis of the 1-Jy sample indicates that the young stellar population and/or AGN is more preeminent in ULIGs than in the lower luminosity objects.

### 3.5. Continuum Colors

The observed continuum colors of the 1-Jy ULIGs are presented in Figure 10 as a function of spectral type. Seyfert 1s have continuum colors (median C6563/C4861 of 0.70) which are significant bluer than all other classes of objects (median C6563/C4861 = 0.98, 1.01, and 1.15 for H II galaxies, LINERs, and Seyfert 2 galaxies, respectively). This result is consistent with the

presence in Seyfert 1s of an AGN emitting a strong energetic continuum. Figure 10 also shows that the optical continuum of ULIGs is on average bluer than that of the BGS LIGs ( $P[\text{null}] = 2 \times 10^{-7}$  when considering all objects). This is especially evident among the LINERs ( $P[\text{null}] = 4 \times 10^{-5}$ ) and the H II galaxies ( $P[\text{null}] = 2 \times 10^{-3}$ ). These results confirm the presence of a strong blue featureless continuum from a young stellar population and/or AGN in the high-luminosity objects (§3.4).

The expected continuum color, C6563/C4861, of galaxies where  $\sim 10\%$  of the galaxy mass has taken part in a burst of star formation less than a few  $10^7$  yrs ago is  $\sim 0.90$  (e.g., Bica, Alloin, & Schmidt 1990). Yet, the continuum colors measured in ULIGs generally are redder than this value. This is a sign that the continuous emission from these objects is probably affected by dust obscuration. However, if the observed continuum colors are dereddened using the amount of dust derived from the emission-line spectrum (§3.2), a strong *negative* correlation becomes apparent between the dereddened continuum colors and dereddened  $H\alpha$  luminosities ( $P[\text{null}] = 10^{-14}$  for the whole sample; in contrast,  $P[\text{null}] = 0.1$  when the *observed* continuum colors are considered). As mentioned in KVS, this result strongly suggests that this dereddening method overcorrects for reddening in the continuum (cf. also §3.7). The emission-line gas near hot stars or the AGN are therefore dustier than the relatively cold stellar population which is producing the optical continuum. This discrepancy is also observed among optically-selected starbursts (e.g., Calzetti et al. 1994; Gordon, Calzetti, & Witt 1997). We have no easy way to properly deredden the continuum colors of our sample galaxies. The dereddened continuum colors will not be considered any further in the present discussion.

### 3.6. $H\alpha$ Luminosities and Equivalent Widths

Here again, many of the conclusions based on the smaller sample of KVS are confirmed in the complete 1-Jy sample. The distributions of  $H\alpha$  equivalent widths, observed  $H\alpha$  luminosities, and infrared-to- $H\alpha$  luminosity ratios are plotted in Figures 11 – 13 for each spectral type. The large  $H\alpha$  luminosities and equivalent widths and small infrared-to- $H\alpha$  luminosity ratios among the (4) Seyfert 1 ULIGs [their median  $EW(H\alpha)$  in  $\text{\AA}$ ,  $\log(L_{H\alpha}/L_{\odot})$ , and  $\log(L_{\text{ir}}/L_{H\alpha})$  are 234, 8.6, and 3.8, respectively] again suggest the presence of an additional source of ionization (AGN) which is not visible or present in starburst-powered galaxies. LINER ULIGs appear to be slightly deficient in  $H\alpha$  relative to H II and Seyfert 2 ULIGs: the median  $\{EW(H\alpha)$  in  $\text{\AA}$ ,  $\log(L_{H\alpha}/L_{\odot})\}$  are  $\{88, 7.8\}$ ,  $\{50, 7.4\}$ , and  $\{84, 7.9\}$  for H II galaxies (30 objects), LINERs (43), and Seyfert 2 galaxies (22), respectively. The observed infrared-to- $H\alpha$  luminosity ratios in LINER ULIGs are also somewhat larger than those of Seyfert 2 and H II ULIGs [median  $\log(L_{\text{ir}}/L_{H\alpha}) = 4.2, 4.7,$  and  $4.2$  for the H II (29), LINER (38), and Seyfert 2 galaxies (21), respectively], confirming the  $H\alpha$  deficiency in LINERs. This deficiency persists even after correcting the emission-line fluxes for reddening using the color excesses derived from the optical Balmer decrements. The  $H\alpha$  equivalent widths of H II and LINER ULIGs are slightly larger than those found in LIGs of the same type (55

Å in HII galaxies and 29 Å in LINERs). This is consistent with the presence of a more preeminent starburst in these ULIGs (§3.4 and §3.5).

### 3.7. Infrared Spectral Properties

The infrared spectral properties of the various classes of LIGs were investigated. We used the definitions of Dahari & De Robertis (1988) for the “*IRAS* color indices” and “infrared color excess” [ $\alpha_1 = -\log(f_{60}/f_{25})/\log(60/25)$ ,  $\alpha_2 = -\log(f_{100}/f_{60})/\log(100/60)$ ,  $IRCE = ((\alpha_1 + 2.48)^2 + (\alpha_2 + 1.94)^2)^{0.5}$ ]. The infrared color excess is a measure of the deviation from colors of non-active spiral galaxies ( $\alpha_1 = -2.48$  and  $\alpha_2 = -1.94$ ; Sekiguchi 1987).

As described in Kim & Sanders (1998), the *IRAS* 60-to-100 flux ratios were used to pre-select the targets for the 1-Jy sample. Consequently, the 1-Jy ULIGs have median  $\alpha_2$  and *IRCE* (−0.41 and 1.63, respectively) which are significantly larger than those of the BGS LIGs (−0.77 and 1.19, respectively), while the median  $\alpha_1$  for ULIGs and BGS LIGs (−2.31 and −2.46, respectively) are similar. The differences in *IRAS* colors between ULIGs and normal galaxies are especially striking among Seyfert 1 galaxies (median  $\alpha_1$ ,  $\alpha_2$ , and *IRCE* of −1.70, +0.05, and 2.16, respectively) and Seyfert 2 galaxies (−2.27, −0.38, and 1.61). The infrared spectral properties of the LINER ULIGs (−2.49, −0.53, and 1.53) are indistinguishable from those of HII ULIGs (−2.49, −0.45, 1.59) and are closer to the parameters of normal spiral galaxies. Therefore, there is no convincing optical or infrared evidence for an AGN in LINER ULIGs. VKSMS and KVS argue that hot stars and/or shocks are the most likely sources of ionization in these objects (cf. §4).

Optically classified H II galaxies in our sample show correlations between infrared colors and H $\alpha$  equivalent widths. H II galaxies with large H $\alpha$  equivalent widths tend to have small  $f_{12}/f_{25}$  and large  $f_{25}/f_{60}$  and  $f_{60}/f_{100}$  (P[null] = 0.001, 0.002 and  $4 \times 10^{-9}$ , respectively; Fig. 14). Similar correlations were reported by Mazzarella, Bothun, & Boroson (1991) among optically-selected starburst galaxies. These results suggest that the most active or youngest star-forming regions produce far-infrared emission with the warmest dust temperatures (Mazzarella et al. 1991). The fact that these correlations are considerably weaker among the infrared-selected Seyfert 2 galaxies (P[null] = 0.11, 0.005 and 0.002, respectively) is another indication that star formation may not be the only source of energy in these objects.

As shown in Figure 15, the well-known correlation between the optical-to-infrared luminosity ratio and the infrared luminosity or *IRAS* flux ratio  $f_{60}/f_{100}$  among luminous infrared galaxies (e.g., VKSMS) disappears when the 1-Jy ULIGs are included in the analysis. In this figure, the optical continuum luminosity, L(4861), is defined as  $P(4861) \times 4861$  where  $P(4861)$  is the monochromatic power of the continuum at 4861 Å. No reddening correction was applied to the continuum luminosity. Note that L(4861) refers to the nuclear region while  $L_{\text{ir}}$  and  $f_{60}/f_{100}$  are integrated quantities. Integrated continuum luminosities are not yet available for most of these galaxies. However, recent imaging studies at infrared and millimeter wavelengths (e.g., Evans 1998; Egami

1998; Scoville et al. 1998; Downes & Solomon 1998; Sakamoto et al. 1999) now strongly suggest that the active regions in ULIGs are generally centered on the inner kpc of the galactic nuclei, with the rest of the galaxy contributing very little to the bolometric luminosity (the situation is different in objects of lower luminosities). The correlations among lower luminosity objects have been interpreted in the past as an indication that high global dust temperature is associated with large infrared dust emission and small optical continuum extinction. The tendency reported by VKSMS for the color excess of H II and LINER LIGs from the BGS sample to decrease at large  $\log L(4861)/L_{ir}$  is consistent with this hypothesis, but this tendency disappears when the 1-Jy ULIGs are included in the analysis. It is not clear at present why that is the case. An attempt to correct  $L(4861)/L_{ir}$  for reddening effects using the color excesses determined from the  $H\alpha/H\beta$  flux ratios fails to bring new insight into this issue. Instead, a very strong *positive* correlation between  $E(B-V)$  and  $L(4861)_0/L_{ir}$  ( $P[\text{null}] = 10^{-43}$  when considering all the objects) is created, confirming that the reddening correction derived from the emission lines severely overestimates the actual extinction of the optical continuum (§3.5).

#### 4. Discussion: Nature of the Energy Source

Most of the trends observed by KVS in their subset of 45 galaxies from the 1-Jy sample are confirmed in the present analysis of the entire sample. Most relevant to the question, raised in the Introduction, of the nature of the energy source in ULIGs is the confirmation that Seyfert 1 or 2 spectral characteristics are present in  $\sim 30\%$  of all ULIGs in the 1-Jy sample, and in  $\sim 50\%$  of the high-luminosity objects ( $\log[L_{ir}/L_{\odot}] > 12.3$ ). The weaker  $H\beta$  and Mg Ib stellar absorption features, bluer continuum colors, larger  $H\alpha$  luminosities and equivalent widths, smaller infrared-to- $H\alpha$  luminosity ratios, and warmer *IRAS*  $f_{25}/f_{60}$  colors in these Seyferts relative to LINER or H II ULIGs are all consistent with the presence of a genuine AGN in these objects. The absence of correlations between line widths and line ratios (not shown here) argues against the possibility that high-velocity shocks (e.g., Binette, Dopita, & Tuohy 1985; Innes 1992; Dopita & Sutherland 1995) are the dominant source of ionization in these Seyfert 2 ULIGs. The very restrictive range of shock conditions (e.g.,  $V_{\text{shock}} = 300 - 500 \text{ km s}^{-1}$ ) needed to produce the high-excitation spectrum of Seyfert 2 galaxies from high-velocity shocks also is inconsistent with the broad range in line widths observed in these objects (cf. also VKSMS).

Recent near-infrared spectroscopy of 22 optically classified Seyfert 2 galaxies from the 1-Jy sample by VSK97 and VSK99 reveals the presence of broad recombination lines with FWHM  $\gtrsim 2,000 \text{ km s}^{-1}$  or strong high-ionization [Si VI] emission in  $\sim 70\%$  of these objects (especially those with warm *IRAS* 25-to-60  $\mu\text{m}$  colors). The absence of broad features in the profiles of the  $H_2$  lines and forbidden [Fe II]  $\lambda 1.257$  suggests that the broad emission is produced by high-density gas near the nucleus like that in the BLR of AGN rather than by outflowing lower density material in the circumnuclear region. The bright [Si VI] feature detected in these objects is also believed to be a good indicator of AGN activity since this feature has never been detected in starburst galaxies

despite extensive searches (e.g., Marconi et al. 1994). The optical and near-infrared results taken together, therefore suggest that the total fraction of objects in the 1-Jy sample with signs of bonafide AGN is at least  $\sim 20 - 25\%$ , but reaches  $\sim 35 - 50\%$  for those objects with  $\log[L_{\text{ir}}/L_{\odot}] > 12.3$ . Nevertheless, the presence of an AGN in ULIGs does not necessarily imply that AGN activity is the dominant energy source in these objects. A more detailed look at the AGN in these ULIGs is needed to answer this question.

A strong linear correlation has long been known to exist between the continuum (or, equivalently, bolometric) luminosities of broad-line AGN and their emission-line luminosities (e.g., Yee 1980; Shuder 1981; Osterbrock 1989). This correlation has often been used to argue that the broad-line regions in AGN are photoionized by the nuclear continuum. If this is the case, the broad-line-to-bolometric luminosity ratio is a measure of the covering factor of the BLR (e.g., Osterbrock 1989). This correlation was also used by VSK97 to estimate the importance of the AGN in powering ULIGs. In ULIGs powered uniquely by an AGN, we expect the broad-line luminosities to fall along the correlation for AGN. Any contribution from a starburst will increase the bolometric luminosity of the ULIG without a corresponding increase in the broad-line luminosity. Starburst-dominated ULIGs are therefore expected to fall below the “pure-AGN” correlation traced by the optical quasars in a diagram of  $L_{\text{H}\beta}(\text{BLR})$  plotted as a function of  $L_{\text{bol}}$ <sup>7</sup>.

In Figure 16, the dereddened *broad-line*  $\text{H}\beta$  luminosities of the Seyfert 1 ULIGs in our sample are plotted as a function of their bolometric luminosities. Data on optically selected quasars and on ULIGs with obscured BLRs (i.e. “buried quasars” detected at near-infrared wavelengths by VSK97) are shown for comparison.  $L_{\text{bol}}$  for the QSOs was determined using the bolometric correction factor 11.8 (i.e.  $L_{\text{bol}} = 11.8\nu_{\text{B}}L_{\nu}(B)$ ): Elvis et al. 1994; Sanders & Mirabel 1996), except for those few sources that were detected by *IRAS*, in which case  $L_{\text{bol}}$  was taken from Sanders et al. (1989). For the 15 ULIGs  $L_{\text{bol}}$  was taken to be  $1.15 \times L_{\text{ir}}$  (Kim & Sanders 1998). The  $\text{H}\beta$  data for the optically selected QSOs are from Yee (1980) corrected for  $H_0 = 75 \text{ km s}^{-1} \text{ Mpc}^{-1}$  and  $q_0 = 0$ . The  $\text{H}\beta$  luminosities tabulated in Yee (1980) include a contribution from narrow  $\text{H}\beta$  and are not corrected for reddening. The flux from narrow  $\text{H}\beta$  is often difficult to measure in these broad-line objects, but the high-quality rest-frame optical spectra that exist on a few of these quasars show that  $L_{\text{H}\beta}(\text{NLR})/L_{\text{H}\beta}(\text{BLR})$  is generally much less than  $\sim 30\%$  (e.g., Boroson & Green 1992; Corbin & Boroson 1996). This correction would lower the quasar data points in Figure 16. The reddening correction to the broad-line luminosities would, on the other hand, raise these data points. The reddening towards the BLRs of these *optically-selected* objects is likely to be modest. In the end, no attempt was made to correct for narrow-line contamination or reddening effects. The best log-linear fit through the quasar data points,  $\log L_{\text{H}\beta}(\text{BLR}) = 1.05$

---

<sup>7</sup>Note that the origin of the far-infrared/submm emission in optical quasars is still a matter of some debate. Some of it may be produced by a dusty circumnuclear starburst (e.g., Rowan-Robinson 1995). In the following discussion, we identify the “pure-AGN”  $L_{\text{H}\beta}(\text{BLR}) - L_{\text{bol}}$  relation as the one traced by optical quasars. We therefore implicitly assume that all of the far-infrared/submm emission is powered by the central AGN (Sanders et al. 1989). The far-infrared/submm emission generally contributes about 20% of the total bolometric luminosities of optical quasars.

$\log L_{\text{bol}} - 3.61$ , is shown as a solid line in Figure 16. The broad-line  $H\beta$  luminosities of the ULIGs with optical BLRs were dereddened using the broad-line  $H\alpha/H\beta$  ratio and assuming an intrinsic ratio of 3.1 (see MacAlpine 1981 for uncertainties associated with using this dereddening method for BLRs). The broad-line  $H\beta$  luminosities of the ULIGs with obscured BLRs were calculated from the measured broad  $\text{Pa}\alpha$  fluxes assuming Case B recombination (except for Mrk 463E = F13536+1836 where the broad  $\text{Pa}\beta$  flux was used). The reddening correction for these objects was carried out using the color excesses derived from the infrared broad-line ratios (cf. VSK97).

Considering the various sources of uncertainties in the derivations of the dereddened broad-line luminosities plotted in Figure 16 (overall uncertainties of order 30%) and the intrinsic scatter of the quasar data points around the “pure” quasar relation (of order 0.2 dex in  $\log[L_{\text{bol}}]$ ), caution should be used when using this figure to make quantitative statements about the dominant energy source in these objects. The positions of 6 or 7 of the 10 optical BLRs (Mrk 231 = F12540+5708, F07599+6508, F13218+0552, F13342+3932, F15462-0450, F21219-1757 and perhaps also Mrk 1014 = F01572+0009) and of all 5 obscured BLRs (Mrk 463E, PKS 1345+12, F20460+1925, F23060+0505, and F23499+2423) fall close (or above) to that of optical quasars in Figure 16. This result suggests that a substantial fraction of the luminosity in these objects is powered by a quasar rather than a starburst. The only broad-line ULIGs which clearly fall below the “pure-AGN” correlation in Figure 16 are NGC 7469, F11119+3257, and F11598-0112. NGC 7469 has long been known to host a Seyfert 1 nucleus and a powerful circumnuclear starburst (De Robertis & Pogge 1986; Wilson et al. 1986). Recent ISO results (Genzel et al. 1998) indicate that the starburst is indeed the dominant infrared energy source in this object. The only other broad-line 1-Jy ULIGs in common with the ISO sample are Mrk 231, Mrk 463E and F23060+0505. In all three cases, the results from the ISO survey support our conclusion that the dominant source of infrared radiation is a quasar rather than a starburst (Genzel et al. 1998).

It is also instructive to study the mid-infrared results on the optically classified LINERs of our sample. Five of these objects were studied by Genzel et al. (1998; UGC 5101, F12112+0305, F14348-1447, F15250+3609, and Arp 220 = F15327+2340). All of them are considered powered predominantly by a starburst (Genzel et al. 1998). This result is also confirmed when a larger sample of ULIGs is considered: if at all present, the AGN in ULIGs with optical LINER characteristics does not appear energetically important in the great majority of these objects (Lutz, Veilleux, & Genzel 1999).

Another method commonly used to estimate the importance of the AGN in ULIGs is based on the strength of the hard (2 – 10 keV) X-ray emission from these objects. Nakagawa et (1998) have recently summarized the ASCA results on ULIGs. Among our subset of broad-line ULIGs, three objects were observed by ASCA: Mrk 231, F20460+1925, and F07599+6508. The first two objects show clear signs of AGN activity in the hard X-rays while the last object was not detected by ASCA. Assuming a X-ray luminosity fraction  $L(2 - 10 \text{ keV})/L_{\text{FIR}} \sim 0.1$  for typical optical quasars, Nakagawa et al. concluded that the AGN contribution to the total luminosity is significant in F20460+1925, in agreement with our optical data, but is small in Mrk 231 and F07599+6508, in

contrast to the optical results (and the ISO results on Mrk 231). A multiwavelength analysis of the Palomar-Green Bright Quasars (Sanders et al. 1989) shows, however, that the X-ray luminosity fraction is typically only about 1% (and can be as small as 0.1% in some objects). The AGN contribution in Mrk 231 would be significant if Mrk 231 happens to lie in the faint X-ray tail of the optically selected quasars. The same conclusion applies to F07599+6508 if the actual hard X-ray flux from this object is close to the upper limit determined by Nakagawa et al. Consequently, the current X-ray data on the broad-line ULIGs of our sample are not inconsistent with the presence of energetically important AGN in many of these broad-line objects.

High-resolution radio observations of several ULIGs have provided additional information on the nature of the energy source of ULIGs. A good correlation seems to exist between the core radio power and bolometric luminosity of optically-selected quasars (Lonsdale, Smith, Lonsdale 1995). This correlation was used by Lonsdale et al. to argue that buried quasars are capable of powering the infrared luminosities in most ULIGs. However, recent VLBI observations by the same group indicate that a starburst may be able to explain the observed radio characteristics of at least a few of these objects (e.g., Arp 220 West; Smith et al. 1998b, Lonsdale et al. 1998). The current VLBI sample includes only two broad-line galaxies from our sample, Mrk 231 and NGC 7469. The VLBI data on these two objects are difficult to explain with a starburst alone, and therefore strongly suggest the presence of an AGN in both objects (Smith et al 1998a). High-resolution radio maps of more broad-line ULIGs from our sample will be needed to properly test our conclusions of the existence of energetically important AGN in these objects.

## 5. Summary

The results from an optical spectroscopic study of the nuclear regions of 108 of the 118 ULIGs from the *IRAS* 1-Jy sample of Kim & Sanders (1998) are reported. These spectra are combined with previously published optical data on 200 LIGs from the BGS sample (VKSMS) to examine the spectral properties of LIGs over the range  $L_{\text{ir}} \approx 10^{10.5} - 10^{13.0} L_{\odot}$ . The results from this analysis confirm many of the trends already seen by KVS in a subset of 45 of these objects. The fraction of LIGs with Seyfert characteristics increases with increasing  $L_{\text{ir}}$ . For  $L_{\text{ir}} > 10^{12.3} L_{\odot}$ , about 48% of the ULIGs (15/31 objects) are classified as Seyfert galaxies. The fraction of Seyfert 1s relative to Seyfert 2s increases with infrared luminosity. This result is not compatible with the predictions of the standard unification model of Seyfert galaxies unless the covering factor of the obscuring material (opening angle of torus?) in Seyfert ULIGs decreases with increasing infrared luminosity.

Many of the optical and infrared spectroscopic properties of the Seyfert galaxies point to the existence of an AGN which is not present or visible in LINER or H II ULIGs. About 30% (10/33) of the Seyfert galaxies in the 1-Jy sample are of type 1, presenting broad Balmer lines and strong Fe II emission similar to what is observed in optically selected quasars. Near-infrared spectroscopy (VSK97, VSK99) often reveals broad (FWHM  $> 2,000 \text{ km s}^{-1}$ ) Paschen emission lines or strong

high-ionization [Si VI] emission in the remaining Seyferts (especially those with warm *IRAS* 25-to-60  $\mu\text{m}$  colors). Seyfert ULIGs (especially those of type 1) have weaker  $\text{H}\beta$  and Mg Ib stellar absorption features, bluer continuum colors, larger  $\text{H}\alpha$  luminosities and equivalent widths, smaller infrared-to- $\text{H}\alpha$  luminosity ratios, and warmer *IRAS*  $f_{25}/f_{60}$  colors than LINER or H II ULIGs. The [O III]  $\lambda 5007$  line widths in the nuclei of the Seyfert galaxies are also significantly broader on average than those measured in the H II and LINER ULIGs.

Comparisons between the emission-line luminosities of the optical or near-infrared broad-line regions in the Seyfert galaxies of the 1-Jy sample and the broad-line luminosities of optical quasars suggest that the AGN in these ULIGs generally is energetically important. Only three objects (NGC 7469, F11119+3257, and F11598-0112) are clearly powered predominantly by a starburst. The general agreement between this optical analysis and the current ISO, X-ray, and VLBI results is encouraging but only based on a limited number of broad-line objects. Results from on-going multiwavelength studies of high-luminosity ULIGs (especially those with  $L_{\text{ir}} \gtrsim 10^{12.3} L_{\odot}$ ) will provide more stringent constraints to test these conclusions.

The weak  $\text{H}\beta$  and Mg Ib features in ULIGs optically classified as H II galaxies or LINERs suggests the presence of a young ( $\lesssim \text{few} \times 10^7$  yrs) stellar population comprising  $\sim 10\%$  of the total galaxy mass in these objects. While this starburst is the likely source of ionization among H II galaxies and some LINERs, long-slit information from VKSMS and KVS indicates that the LINER-like emission may also be produced through shocks caused by the interaction of starburst-driven outflows with the ambient material. Comparisons of the optical results with recent mid-infrared data obtained with ISO suggest that the main source of energy in these infrared-selected H II galaxies and LINERs is a starburst rather than an AGN. The observed continuum colors and strengths of the stellar absorption features and  $\text{H}\alpha$  emission line indicate that the starburst becomes increasingly important with increasing infrared luminosity in both H II galaxies and LINERs.

The large  $\text{H}\alpha/\text{H}\beta$  ratio and red continuum colors of the 1-Jy ULIGs confirm the importance of dust in all these objects. As was found among optically selected starbursts, the relatively cool stars which are producing the continuous optical emission are less reddened than the emission-line gas in ULIGs. No significant differences are found between the mean emission-line color excess of ULIGs and that of *IRAS* galaxies of lower infrared luminosity. The color excess in the nuclei of ULIGs does not depend strongly on the optical spectral type or *IRAS* 25-to-60  $\mu\text{m}$  color. The most likely explanation for this surprising result is that the optical method used to derive the color excess in infrared galaxies underestimates the amount of dust in the dustier, cooler objects.



S. V. and D. B. S. thank the organizers of the 1998 Ringberg meeting where some of the issues in this paper were discussed. We are also grateful to the editor, Dr. Greg Bothun, and the anonymous referee for suggestions which significantly improved this paper. This research was supported in part by JPL contract no. 961566 to the University of Hawaii (D. B. S.). S. V. is grateful for partial support of this research by NASA/LTSA grant NAG 56547 and Hubble fellowship HF-1039.01-92A awarded by the Space Telescope Science Institute which is operated by the AURA, Inc. for NASA under contract No. NAS5-26555. This research has made use of the NASA/IPAC Extragalactic Database (NED) which is operated by the Jet Propulsion Laboratory, California Institute of Technology, under contract with NASA.

## REFERENCES

- Allen, D. A., Norris, R. P., Meadows, V. S., & Roche, P. F. 1991, MNRAS, 248, 528
- Armus, L., Heckman, T. M., & Miley, G. K. 1989, ApJ, 347, 727
- Ashby, M., Houck, J. R., & Hacking, P. B. 1992, AJ, 10, 980
- Ashby, M., Houck, J. R., & Matthews, K. 1995, ApJ, 447, 545
- Bica, E., Alloin, D., & Schmidt, A. 1990, MNRAS, 242, 241
- Boroson, T. A., & Green, R. F. 1992, ApJS, 80, 109
- Calzetti, D., Kinney, A. L., & Storchi-Bergmann, T. 1994, ApJ, 429, 482
- Corbin, M. R., & Boroson, T. A. 1996, ApJS, 107, 69
- Dahari, O., & De Robertis, M. M. 1988, ApJS, 67, 249
- de Grijp, M. H. K., Miley, G. K., Lub, J., & De Jong, T. 1985, Nature, 314, 240
- De Robertis, M. M., & Pogge, R. W. 1986, AJ, 91, 1026
- Downes, D., & Solomon, P. M. 1998, ApJ, 507, 615
- Egami, E. 1998, Ap&SS, submitted (Proceedings of 1998 Ringberg workshop on Ultraluminous Infrared Galaxies)
- Elvis, M. et al. 1994, ApJS, 95, 1
- Evans, A. S. 1998, Ap&SS, submitted (Proceedings of 1998 Ringberg workshop on Ultraluminous Infrared Galaxies)
- Evans, I. N., & Dopita, M. A. 1985, ApJS, 57, 503
- Gaskell, C. M., & Ferland, G. J. 1984, PASP, 96, 393
- Genzel, R., et al. 1998, ApJ, 498, 579
- Gordon, K. D., Calzetti, D., & Witt, A. N. 1997, ApJ, 487, 625
- Halpern, J. P., & Steiner, J. E., ApJ, 269, L37
- Heckman, T. M. 1980, A&A, 87, 152
- Heckman, T. M., Balick, B., & Crane, P. C. 1980, A&AS, 40, 295
- Jacoby, G. H., Hunter, D. A., & Christian, C. A. 1984, ApJS, 56, 256
- Keel, W. C. 1983, ApJ, 269, 466
- Kennicutt, R. C. Jr., Keel, W. C., & Blaha, C. A. 1989, AJ, 97, 1022
- Kim, D.-C. 1995, Ph. D. Thesis, University of Hawaii
- Kim, D.-C., & Sanders, D. B. 1998, ApJS, 119, 41
- Kim, D. -C., Veilleux, S., Sanders, D. B. 1998, ApJ, in press (KVS)
- Kim, D. -C., Veilleux, S., Sanders, D. B., Mazzarella, J. M., & Soifer, B. T. 1995, ApJS, 98, 129

- Leech, K. J., Penston, M. V., Terlvich, R., Lawrence, A., Rowan-Robinson, M. , & Crawford, J. 1989, MNRAS, 240, 349
- Lonsdale, C. J., Lonsdale, C. J., Diamond, P. J., & Smith, H. E. 1998, ApJ, 493, L13
- Lonsdale, C. J., Smith, H. E., & Lonsdale, C. J. 1995, ApJ, 438, 632
- Lutz, D. et al. 1996, A&A, 315, L137
- Lutz, D., Spoon, H. W. W., Rigopoulou, D., Moorwood, A. F. M., & Genzel, R. 1998, ApJ, 505, L103
- Lutz, D., Veilleux, S., & Genzel, R. 1999, ApJ, submitted
- Mazzarella, J. M., Bothun, G. D., & Boroson, T. A. 1991, AJ, 101, 2034
- McCall, M. L., Rybski, P. M., & Shields, G. A. 1985, ApJS, 57, 1
- Miley, G. K., Neugebauer, G., & Soifer, B. T. 1985, ApJ, 293, L11
- Miller, J. S., & Mathews, W. G. 1972, ApJ, 172, 593
- Moshir, M. et al. 1992, Explanatory Supplement to the *IRAS* Faint Source Survey, Version 2, JPL D-10015 8/92 (Pasadena: JPL) (FSC)
- Mulchaey, J. S., et al. 1994, ApJ, 436, 586
- Nakagawa, T., et al. 1998, in proceedings of IAU Symposium #186, Galaxy Interactions at Low and High Redshift, p. 000
- Osterbrock, D. E. 1989. *Astrophysics of Gaseous Nebulae and Active Galactic Nuclei* (Mill Valley: University Science Books)
- Perault, M. 1987, PhD Thesis, University of Paris
- Rowan-Robinson, M. 1995, MNRAS, 272, 737
- Sakamoto, K., Scoville, N. Z., Yun, M. S., Crosas, M., Genzel, R., & Tacconi, L. J. 1999, ApJ, in press
- Sanders, D. B., & Mirabel, I. F. 1996, ARA&A, 34, 725
- Sanders, D. B., Phinney, E. S., Neugebauer, G., & Mathews, K. 1989, ApJ, 347, 29
- Sanders, D. B., Soifer, B. T., Elias, J. H., Madore, B. F., Matthews, K., Neugebauer, G., & Scoville, N. Z. 1988a, ApJ, 325, 74
- Sanders, D. B., Soifer, B. T., Elias, J. H., Neugebauer, G., & Matthews, K. 1988b, ApJ, 328, L35
- Scoville, N. Z., Yun, M. S., & Bryant, P. M. 1997, ApJ, 484, 702
- Sekiguchi, K. 1987, ApJ, 316, 145
- Shuder, J. M. 1981, ApJ, 244, 12
- Smith, H. E., Lonsdale, C. J., & Lonsdale, C. J. 1998a, ApJ, 492, 137
- Smith, H. E., Lonsdale, C. J., Lonsdale, C. J., & Diamond, P. J. 1998b, ApJ, 493, L17

- Soifer, B. T., Boehmer, L., Neugebauer, G., & Sanders, D. B. 1989, *AJ*, 98, 766
- Soifer, B. T., Sanders, D. B., Madore, B., Neugebauer, G., Danielson, G. E., Elias, J. H., Persson, C. J., & Rice, W. L. 1987, *ApJ*, 320, 238
- Stauffer, J. R. 1982, *ApJS*, 50, 517
- Surace, J. A. 1998, Ph. D. Thesis, University of Hawaii
- Surace, J. A., Sanders, D. B., Vacca, W. D., Veilleux, S., & Mazzarella, J. M. 1998, *ApJ*, 492, 116
- Veilleux, S. 1991, *ApJS*, 75, 383
- Veilleux, S., Kim, D. -C., Sanders, D. B., Mazzarella, J. M., & Soifer, B. T. 1995, *ApJS*, 98, 171 (VKSMS)
- Veilleux, S., Kim, C.-C., & Sanders, D. B. 1999a, in preparation
- Veilleux, S., & Osterbrock, D. E. 1987, *ApJS*, 63, 295
- Veilleux, S., Sanders, D. B., & Kim, D.-C. 1997, *ApJ*, 484, 92 (VSK97)
- Veilleux, S., Sanders, D. B., & Kim, D.-C. 1999b, *ApJ*, submitted (VSK99)
- Wilson, A. S., Baldwin, J. A., Sze-Dung, Sun, & Wright, A. E. 1986, *ApJ*, 310, 121
- Yee, H. K. C. 1980, *ApJ*, 241, 894

FIGURE CAPTIONS

Fig. 1.— Optical spectra of the ULIGs in the KPNO sample —  $f_\lambda$  is plotted vs  $\lambda_{\text{observed}}$ . The units of the vertical axis are  $10^{-15} \text{ erg s}^{-1} \text{ cm}^{-2} \text{ \AA}^{-1}$  while the wavelength scale is in  $\text{\AA}$ .

Fig. 2.— Dereddened flux ratios. The H II region-like galaxies (H) are located to the left of the solid curve while LINERs (L) and Seyfert 2 galaxies (S) are located on the right. Seyfert 2 galaxies present  $[\text{O III}]\lambda 5007/\text{H}\beta \geq 3$  (indicated by a solid horizontal segment). Seyfert 1 galaxies are not shown in the diagrams.

Fig. 3.— Summary of the results of the spectral classification as a function of the infrared luminosity. The results from the present paper were combined with those obtained by Veilleux et al. (1995) on LIGs in the BGS. The fraction of Seyferts increases with infrared luminosity.

Fig. 4.— Distribution of the color excesses as a function of spectral types for the ULIGs in the 1-Jy sample (solid line) and the BGS LIGs of Veilleux et al. (1995; dashed line). Both classes of objects present large color excesses. The differences between the various types of ULIGs are not significant.

Fig. 5.— *IRAS* flux density ratios  $f_{25}/f_{60}$  as a function of the color excesses for each spectral type. The stars are the H II galaxies, the open circles are the LINERs, and the filled circles are the Seyfert 2 galaxies. The large symbols are the ULIGs from the 1-Jy sample and the small symbols are the BGS LIGs from Veilleux et al. (1995). No significant correlation is observed.

Fig. 6.— Distribution of the  $[\text{O III}]\lambda 5007$  line widths as a function of the spectral types of the ULIGs in the 1-Jy sample (solid line) and the BGS LIGs of Veilleux et al. (1995; dashed line). The median line widths of H II and LINER ULIGs are significantly smaller than those of Seyfert ULIGs.

Fig. 7.—  $[\text{O III}]\lambda 5007$  line widths as a function of (a) the infrared luminosities and (b) the *IRAS* flux density ratios  $f_{25}/f_{60}$ . Solid squares represent Seyfert 1 galaxies. The meaning of the other symbols is the same as in Fig. 5. The objects with large  $[\text{O III}]$  line widths generally have large infrared luminosities and many of them have Seyfert optical characteristics and warm *IRAS* colors.

Fig. 8.— Distribution of the equivalent widths of  $\text{H}\beta$  in absorption as a function of the spectral types of the ULIGs in the 1-Jy sample (solid line) and the BGS LIGs of Veilleux et al. (1995; dashed line). The equivalent widths of the ULIGs are on average smaller than those of the lower-luminosity objects. Seyfert ULIGs also have somewhat smaller equivalent widths than LINERs and H II galaxies.

Fig. 9.— Distribution of the equivalent widths of  $\text{Mg Ib } \lambda 5176$  as a function of the spectral types of the ULIGs in the 1-Jy sample (solid line) and the BGS LIGs of Veilleux et al. (1995; dashed line).

The equivalent widths of the ULIGs are on average smaller than those of the lower-luminosity objects. Seyfert ULIGs also have somewhat smaller equivalent widths than LINERs and H II galaxies.

Fig. 10.— Distribution of the observed continuum colors, (C6563/C4861), as a function of the spectral types of the ULIGs in the 1-Jy sample (solid line) and the BGS LIGs of Veilleux et al. (1995; dashed line). The nuclear continuum of Seyfert 1 ULIGs is significantly bluer on average than the continuum of all other classes of objects. There is also a tendency for the continuum colors of ULIGs to be bluer on average than those of LIGs.

Fig. 11.— Distribution of the equivalent widths of H $\alpha$  in emission as a function of the spectral types of the ULIGs in the 1-Jy sample (solid line) and the BGS LIGs of Veilleux et al. (1995; dashed line). Note the large equivalent widths of Seyfert 1 galaxies. LINERs have equivalent widths which are somewhat smaller than those of H II galaxies, both at low and high infrared luminosities.

Fig. 12.— Distribution of the observed H $\alpha$  luminosities as a function of the spectral types of the ULIGs in the 1-Jy sample (solid line) and the BGS LIGs of Veilleux et al. (1995; dashed line). Seyfert 1 galaxies are very luminous H $\alpha$  emitters. The LINERs are somewhat underluminous relative to H II and Seyfert 2 galaxies, both at high and low infrared luminosities.

Fig. 13.— Distribution of the observed infrared-to-H $\alpha$  luminosity ratios as a function of spectral types of the ULIGs in the 1-Jy sample (solid line) and the BGS LIGs of Veilleux et al. (1995; dashed line). Seyfert 1s present smaller ratios than any other classes objects; LINERs present slightly larger ratios than H II and Seyfert 2 galaxies.

Fig. 14.— H $\alpha$  equivalent widths as a function of (a) *IRAS* flux density ratio  $f_{12}/f_{25}$ , (b) *IRAS* flux density ratio  $f_{25}/f_{60}$ , and (c) *IRAS* flux density ratio  $f_{60}/f_{100}$ . The meaning of the symbols is the same as in Fig. 7. Correlations are apparent among H II galaxies.

Fig. 15.— Observed optical-to-infrared luminosity ratios as a function of (a) infrared luminosity and (b) *IRAS* flux density ratio  $f_{60}/f_{100}$ . The meaning of the symbols is the same as in Fig. 7. The correlations previously detected among the BGS LIGs are not apparent among the 1-Jy ULIGs.

Fig. 16.— Comparison of the broad-line H $\beta$  luminosities of ULIGs and optically identified QSOs as a function of their bolometric luminosities. The data on the optical quasars are taken from Yee (1980), while the data on ULIGs with obscured broad-line regions are from Veilleux, Sanders, & Kim (1997). See text for a discussion of the methods used to construct this figure. The solid line represents the best log-linear fit through the quasar data points. Given the uncertainties on the broad-line luminosities (about 30%), only three objects from the sample of ten ULIGs with optical broad lines (NGC 7469, F11119+3257, and F11598-0112) clearly fall below the solid line and therefore appear to be powered predominantly by a starburst. The quasar is likely to be the dominant energy source in the other ULIGs.

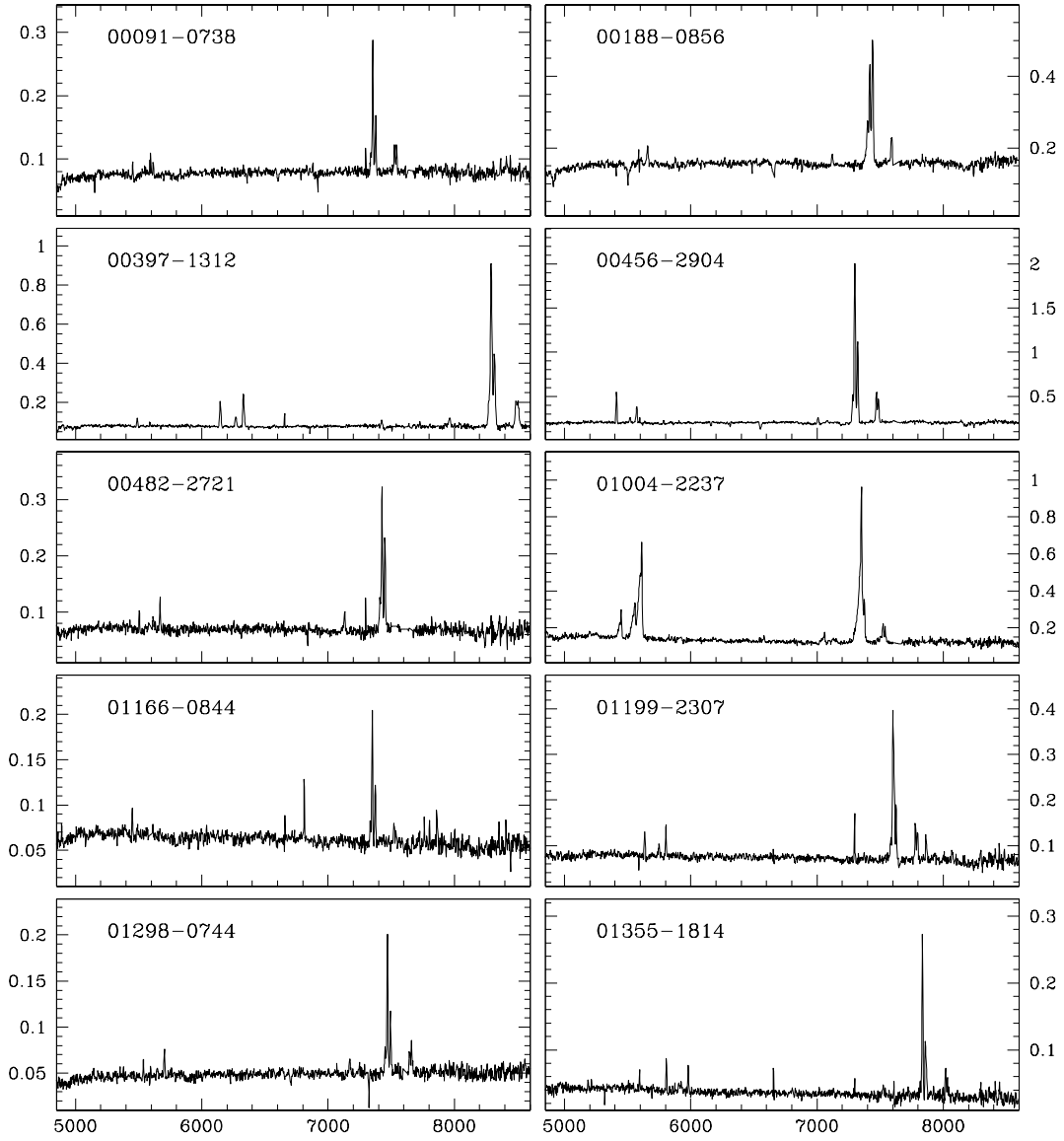


Fig. 1.—

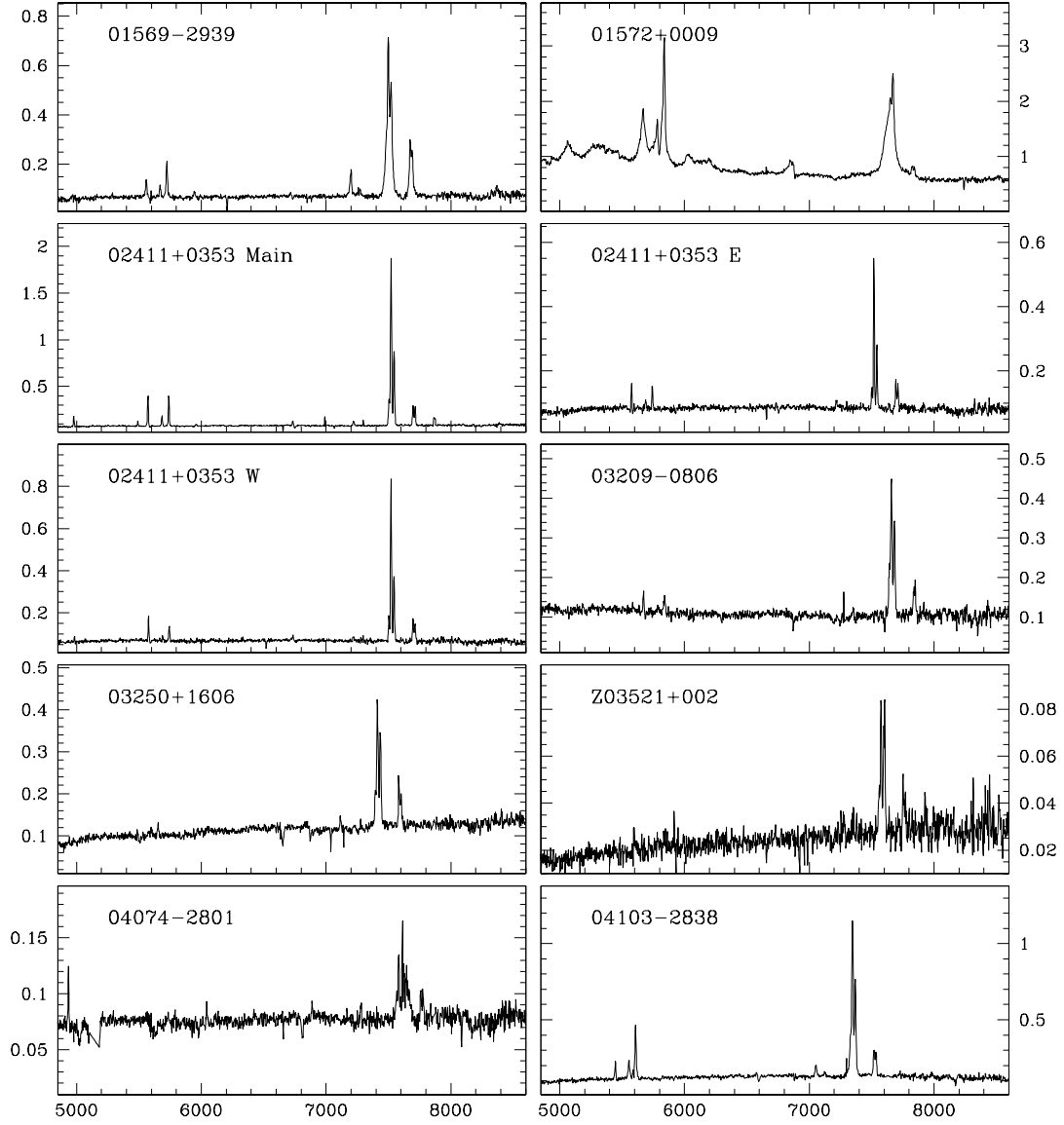


Fig. 1.—



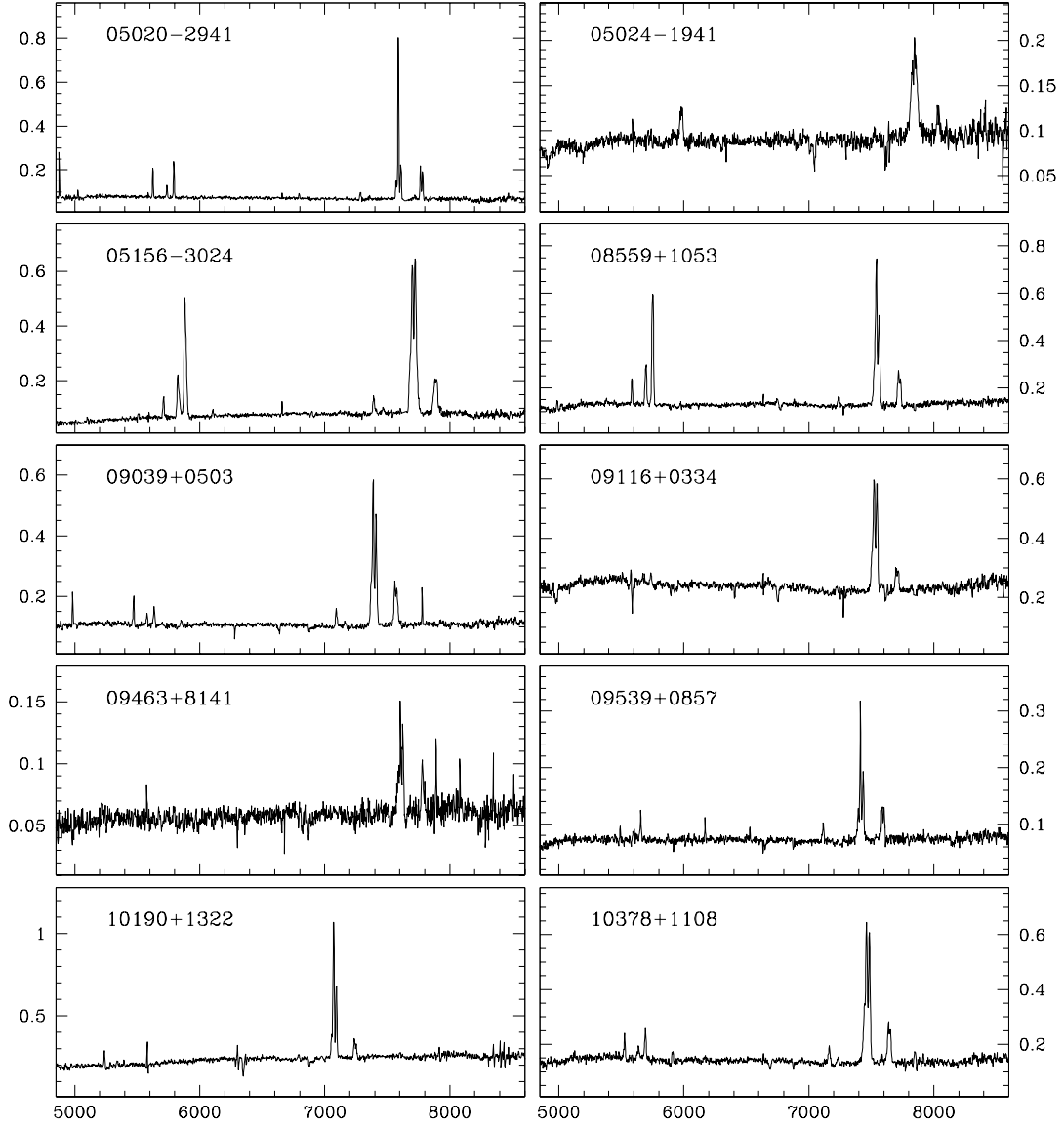


Fig. 1.—

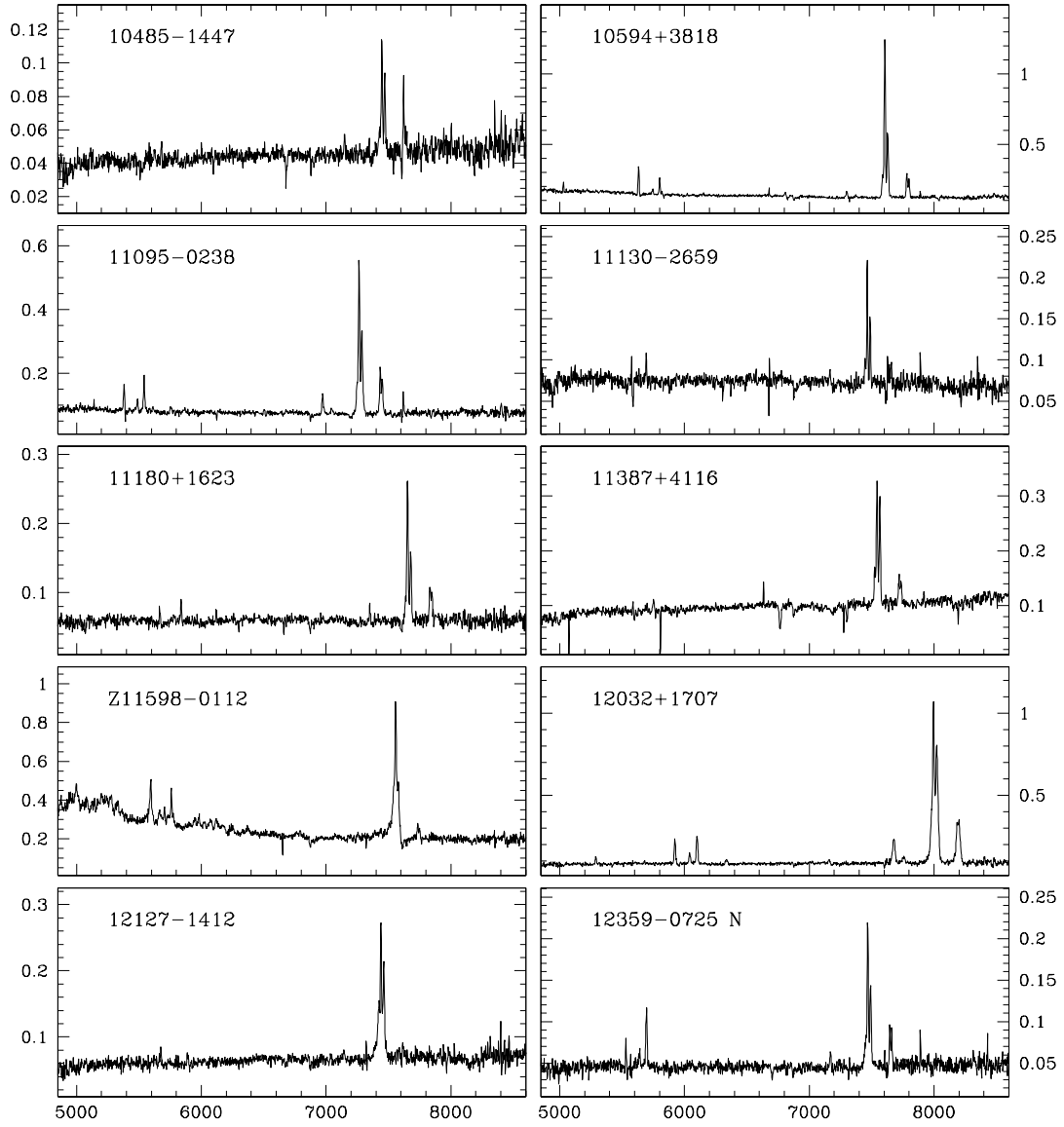


Fig. 1.—

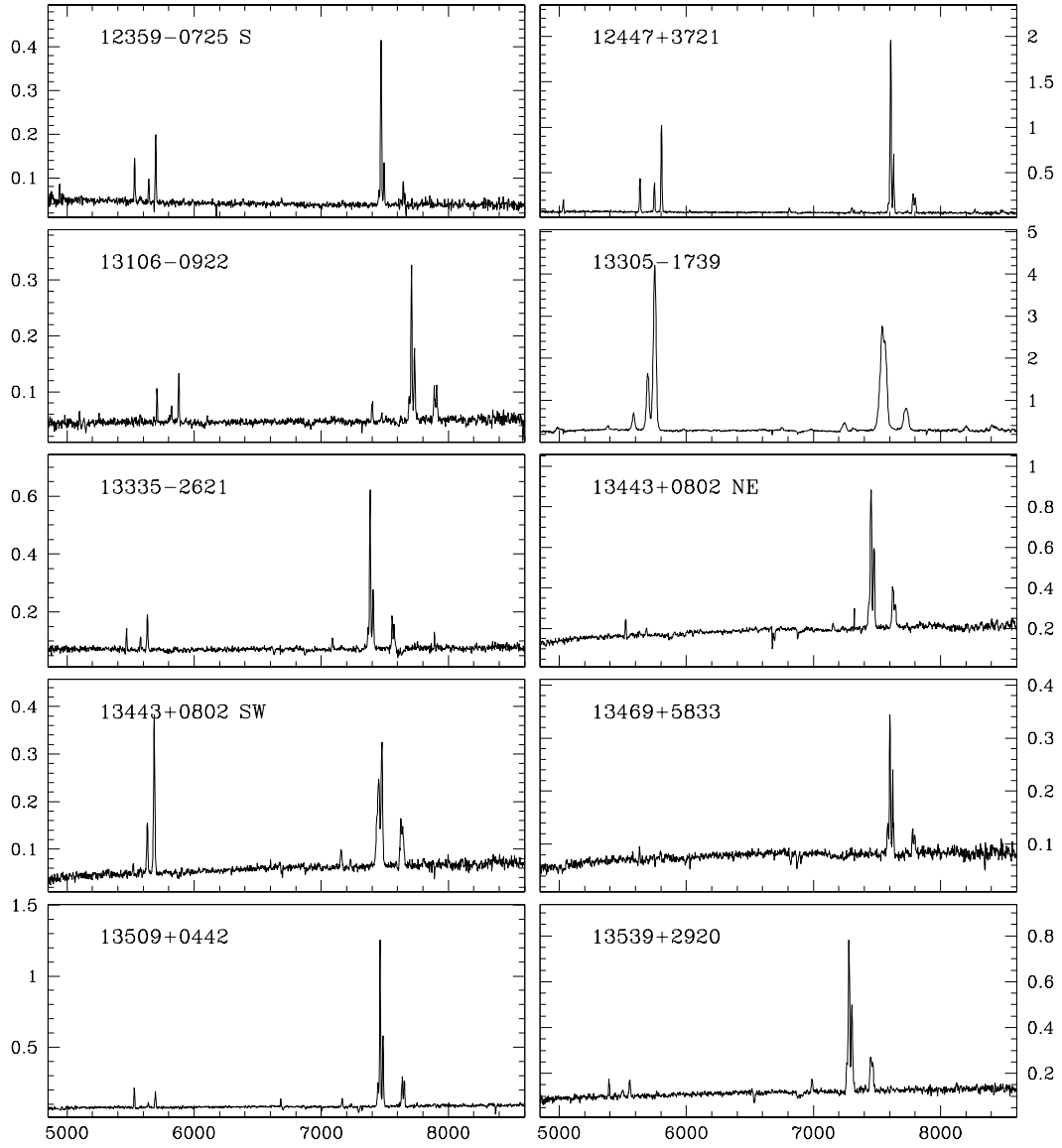


Fig. 1.—

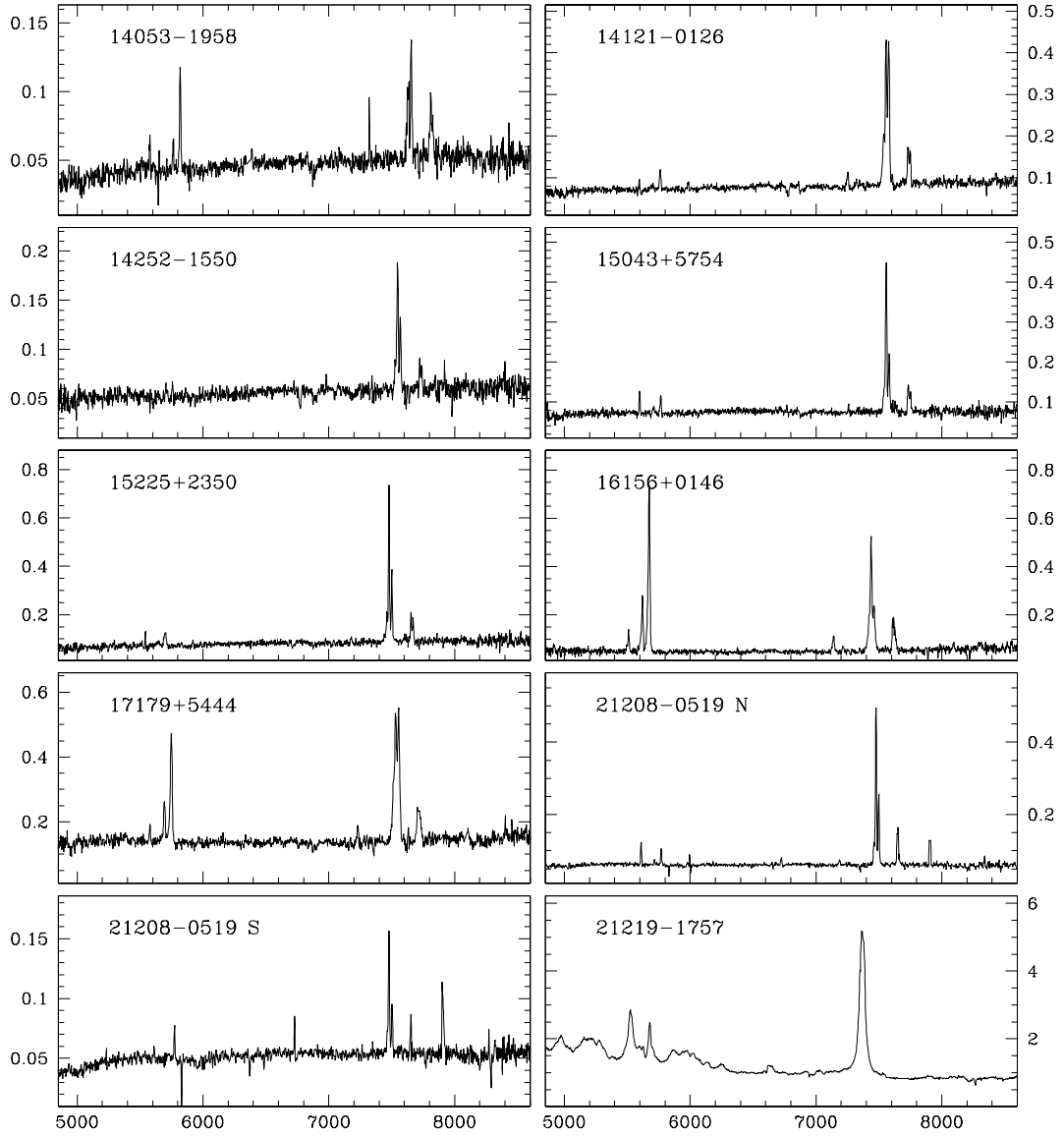


Fig. 1.—

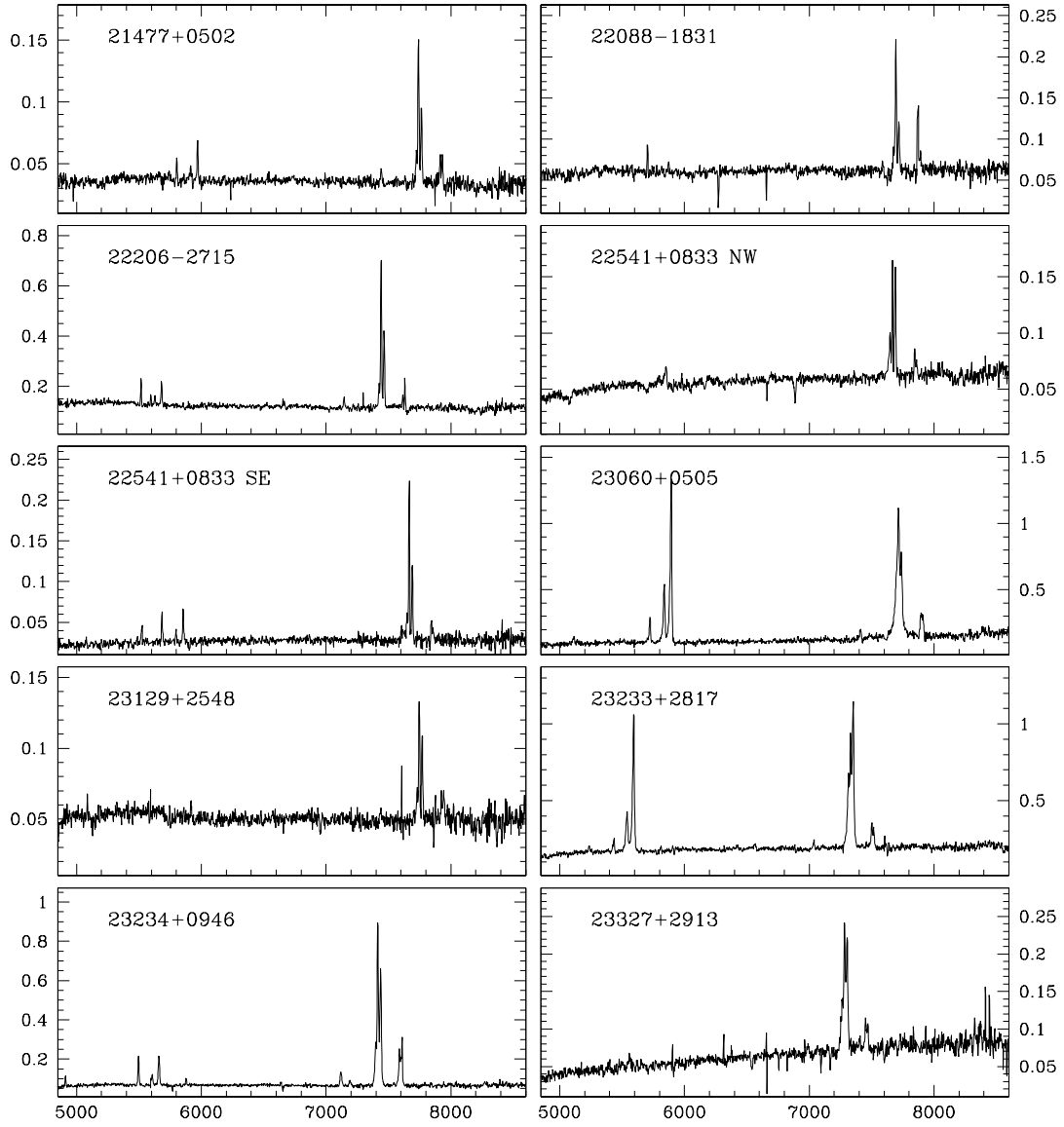


Fig. 1.—

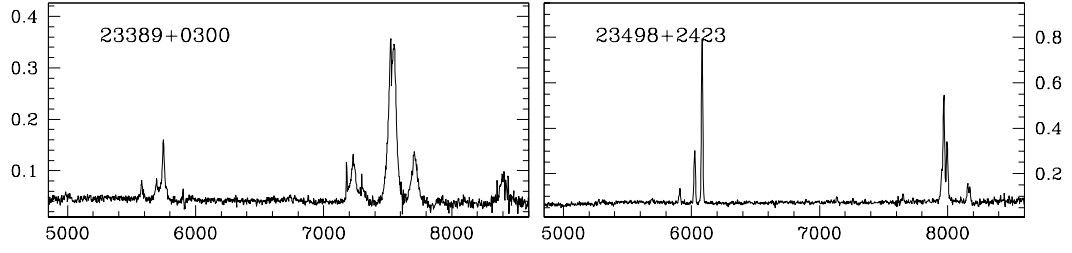


Fig. 1.—

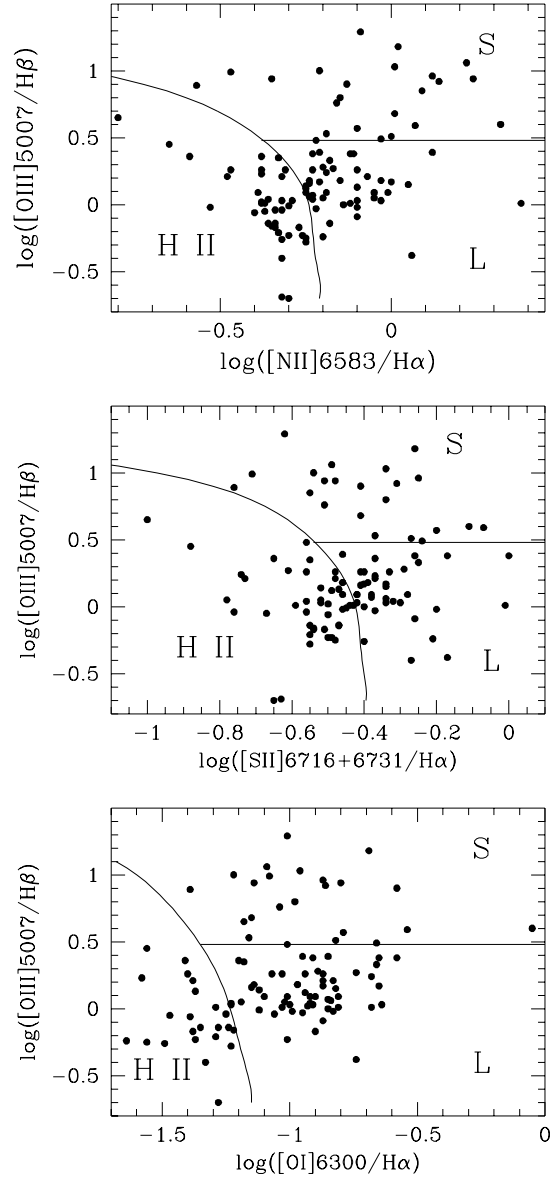


Fig. 2.—

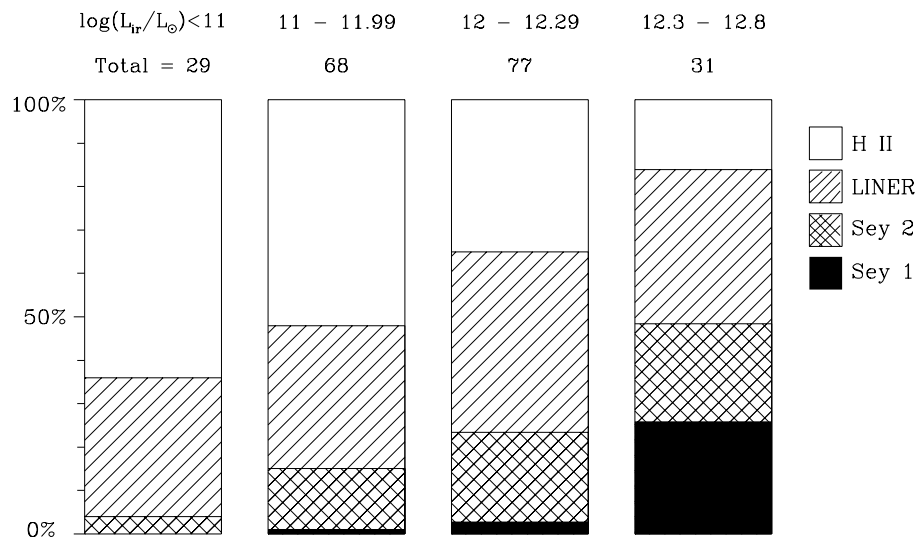


Fig. 3.—



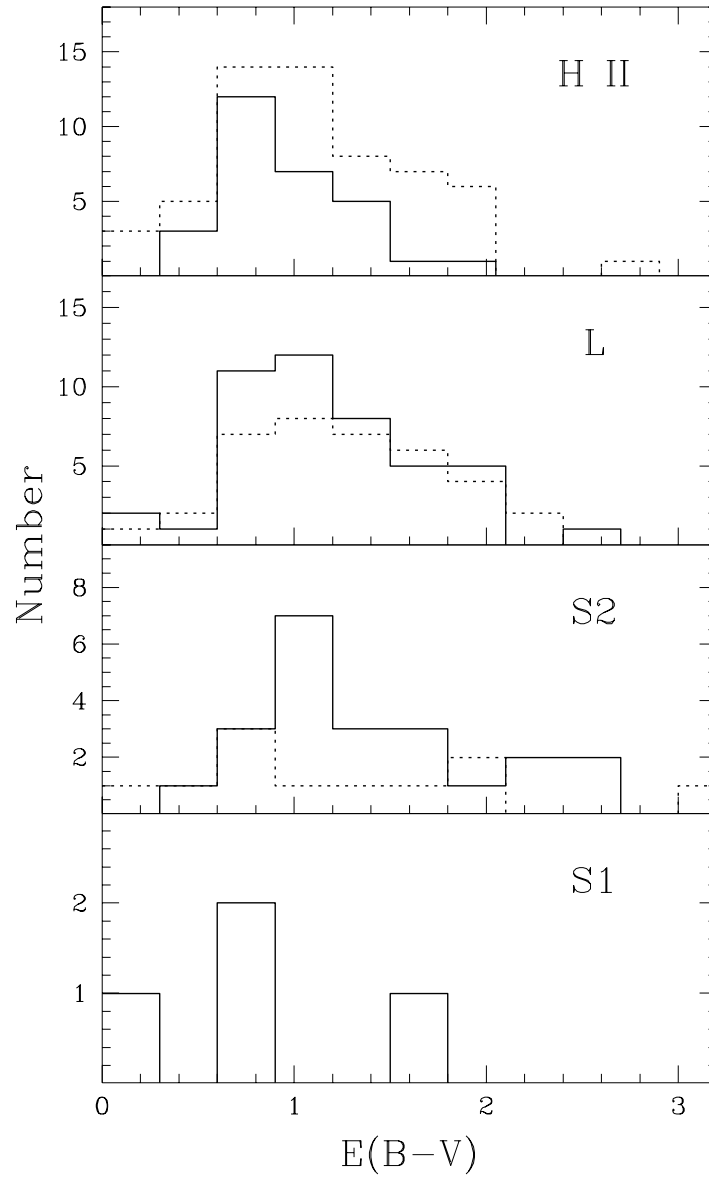


Fig. 4.—

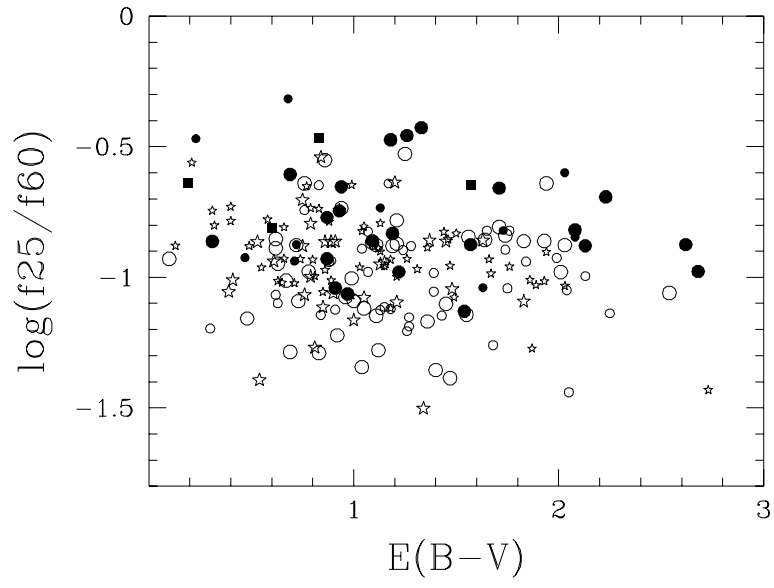


Fig. 5.—

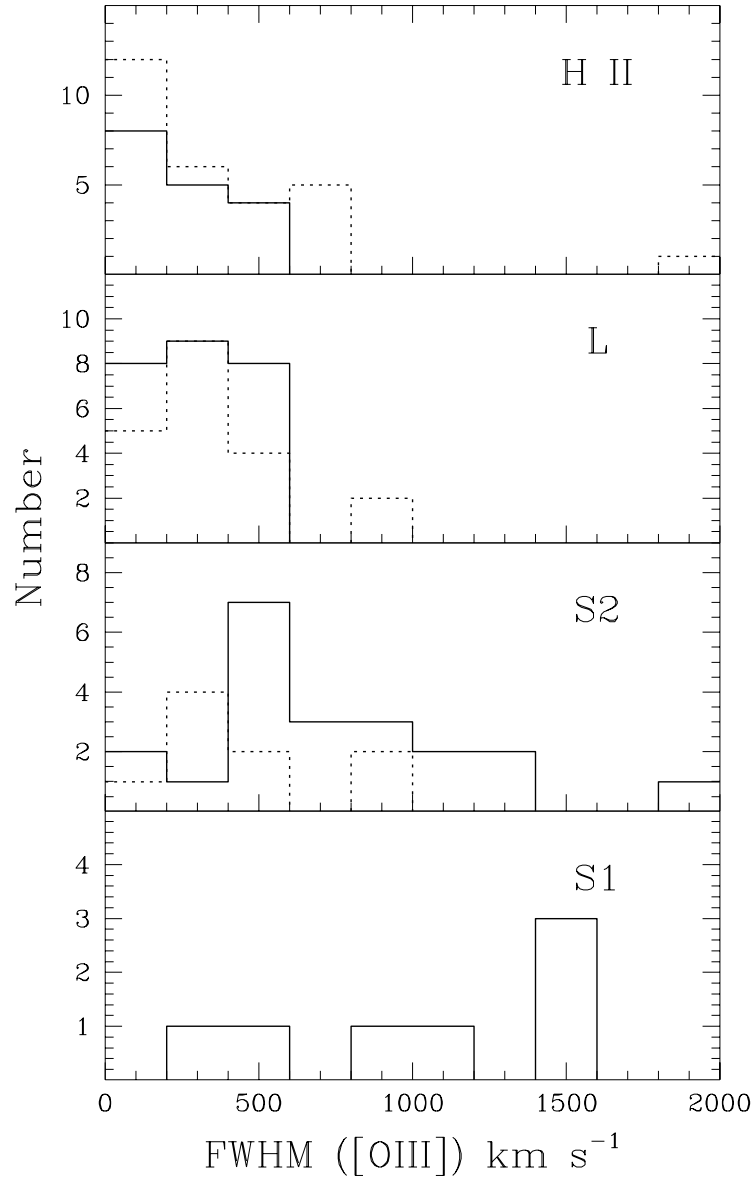


Fig. 6.—

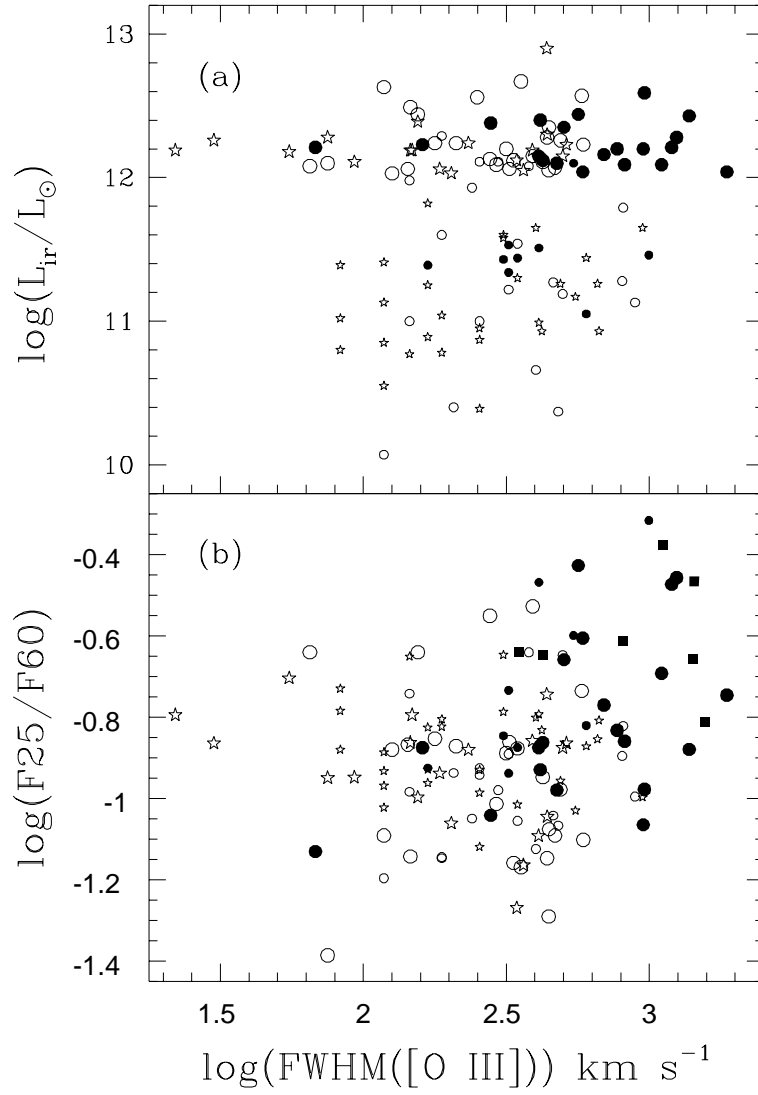


Fig. 7.—

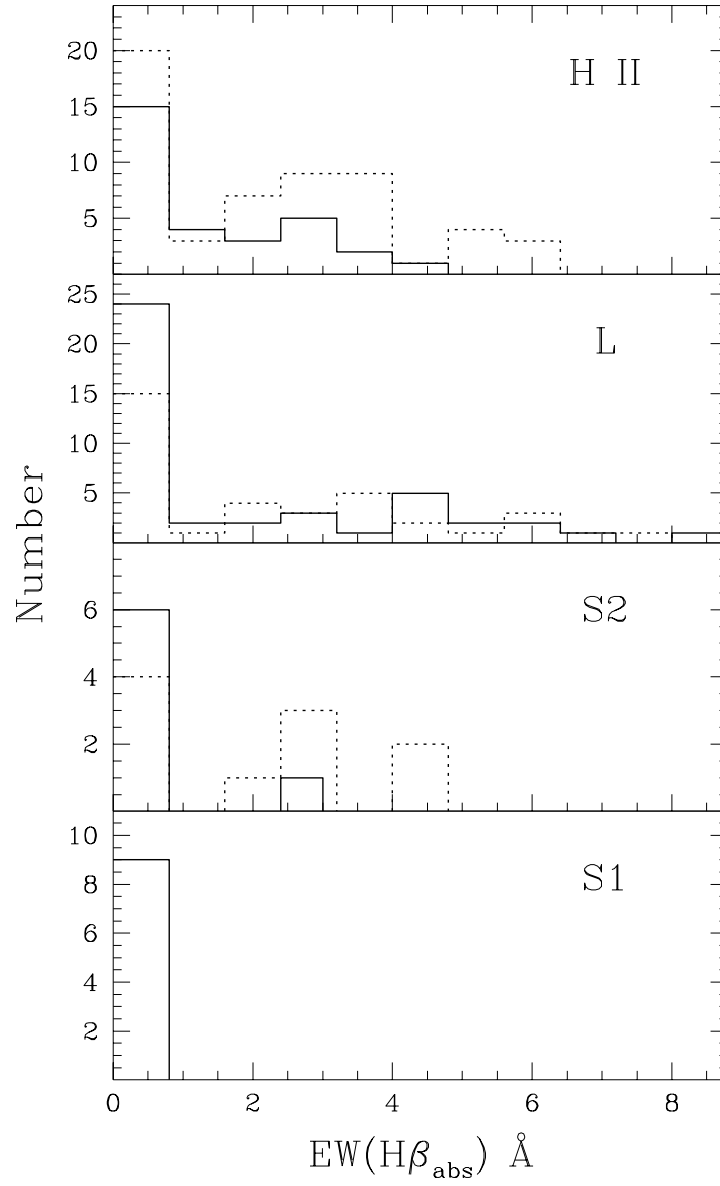


Fig. 8.—

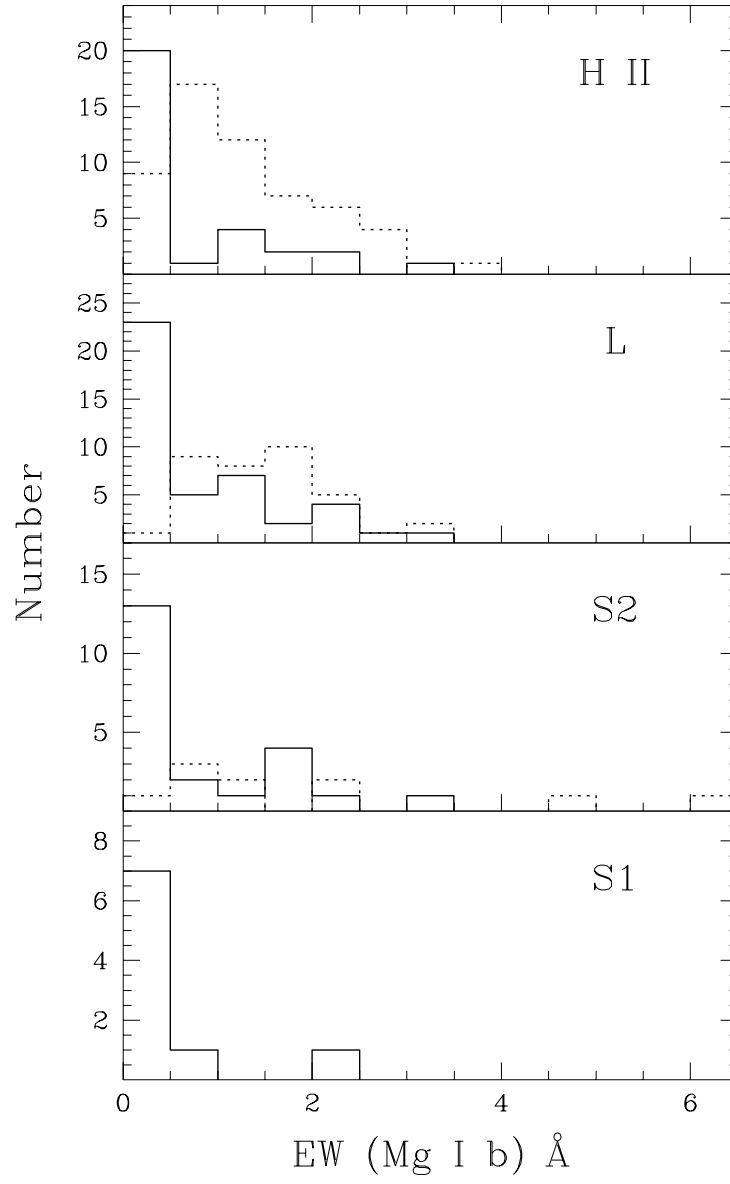


Fig. 9.—

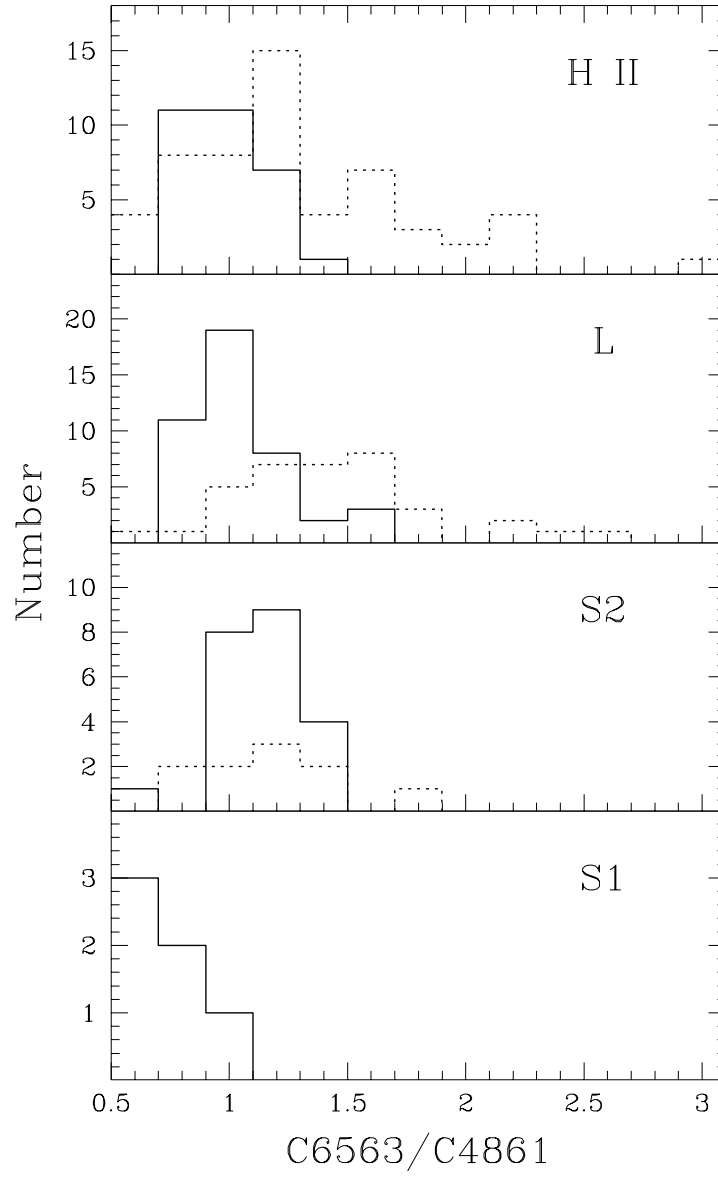


Fig. 10.—

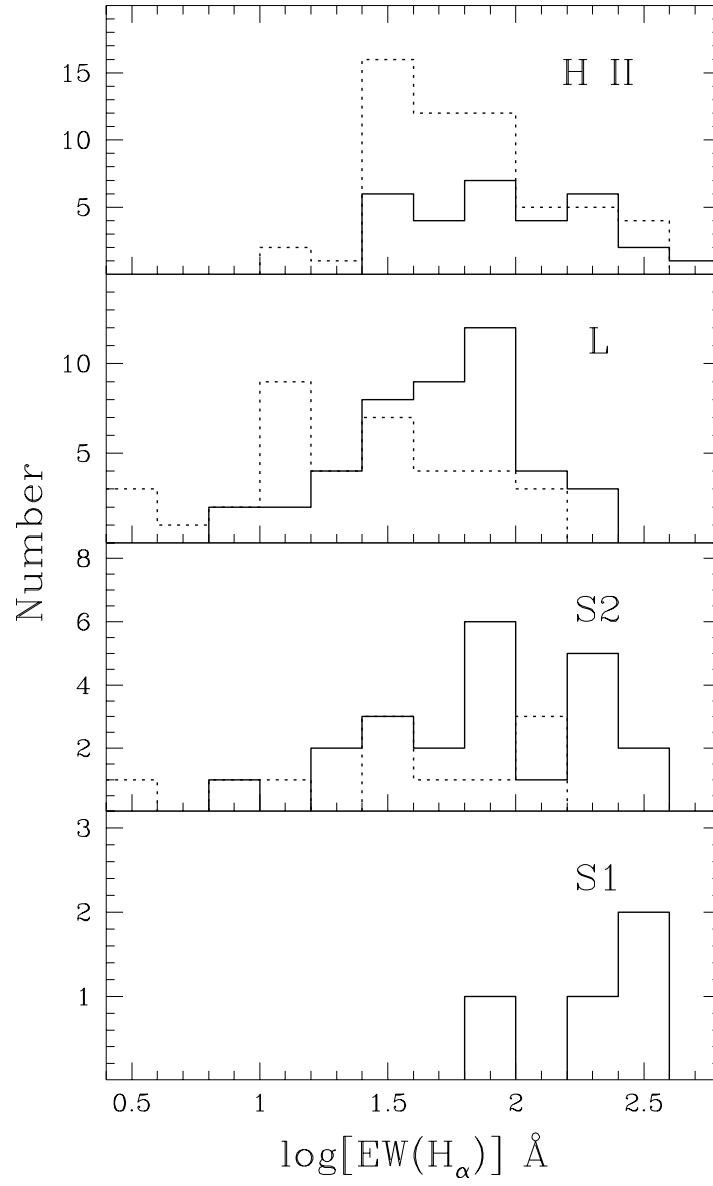


Fig. 11.—



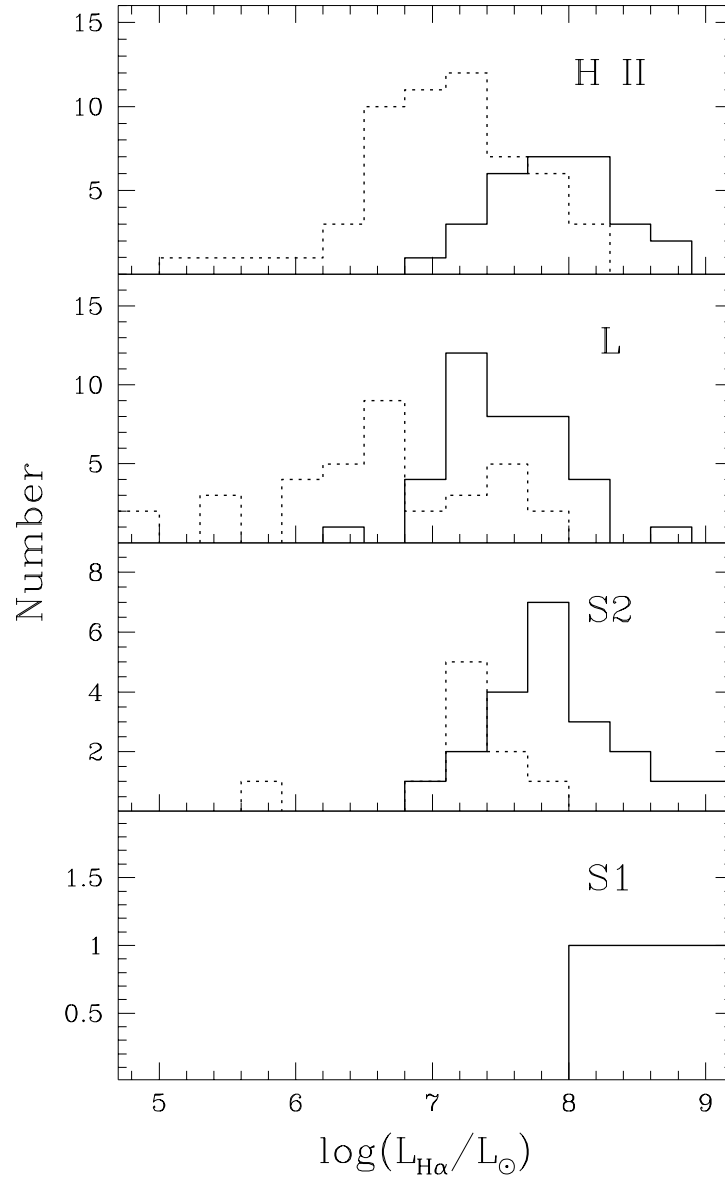


Fig. 12.—

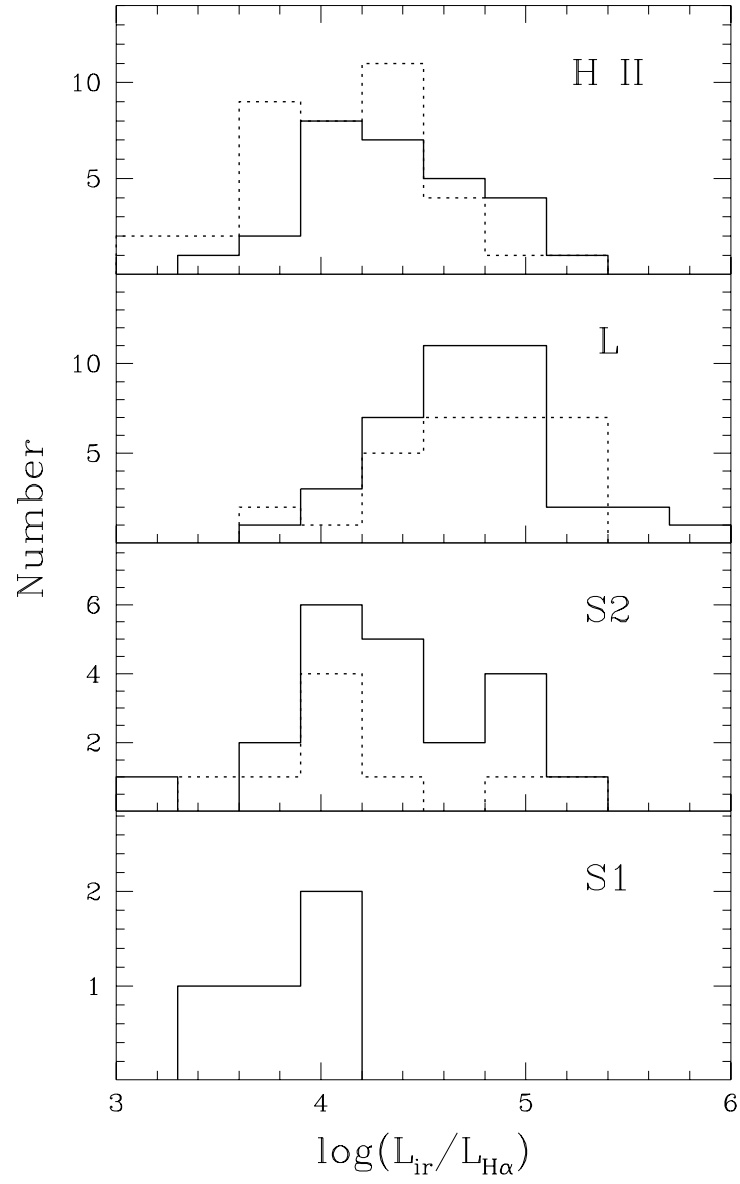


Fig. 13.—

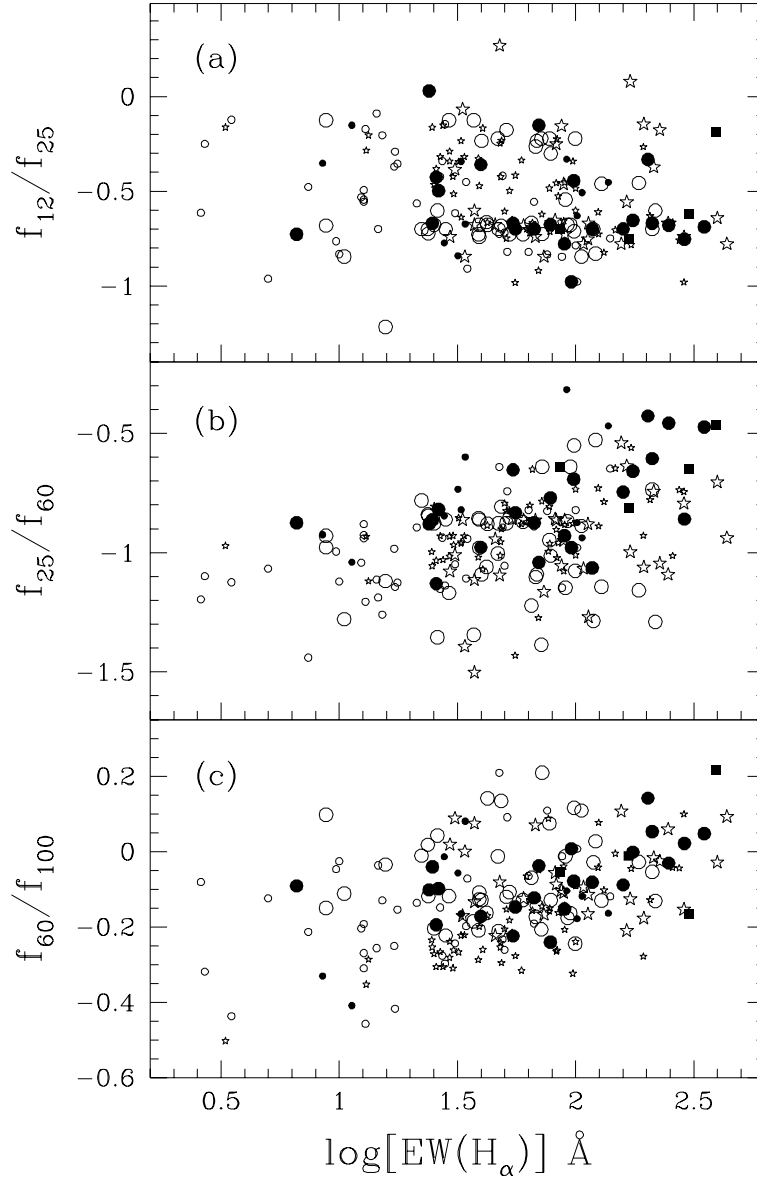


Fig. 14.—

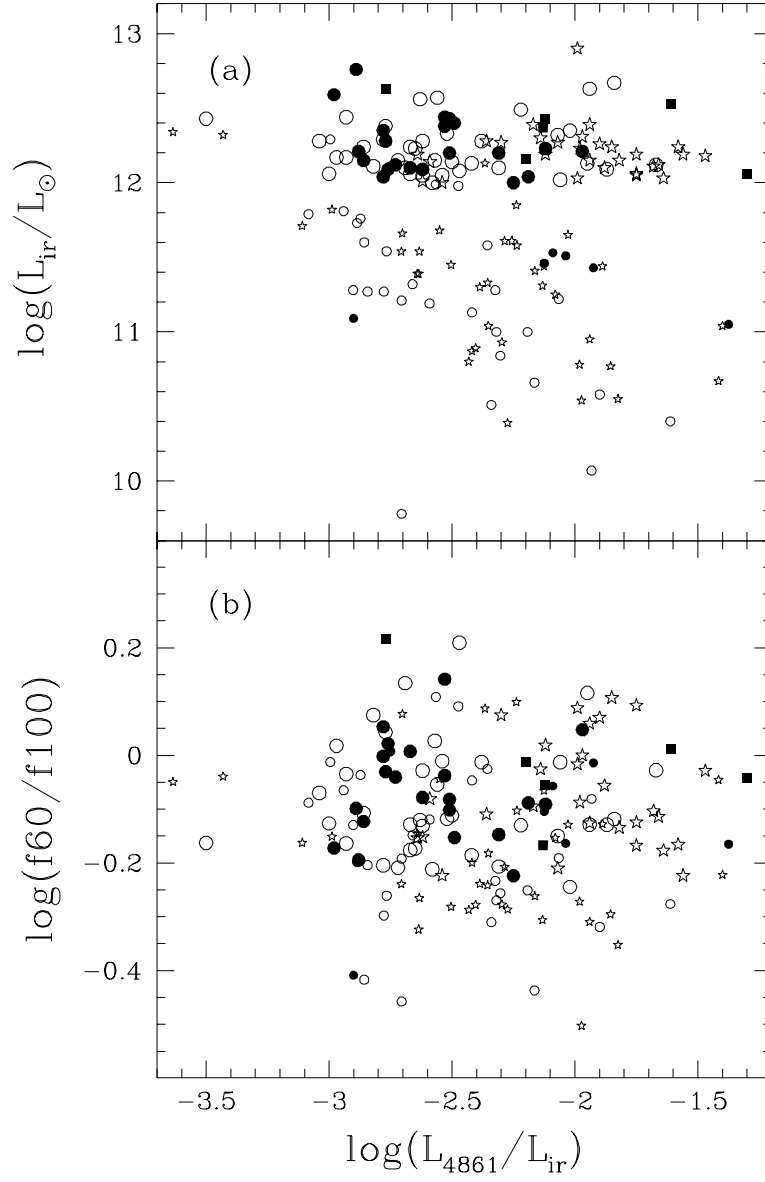


Fig. 15.—

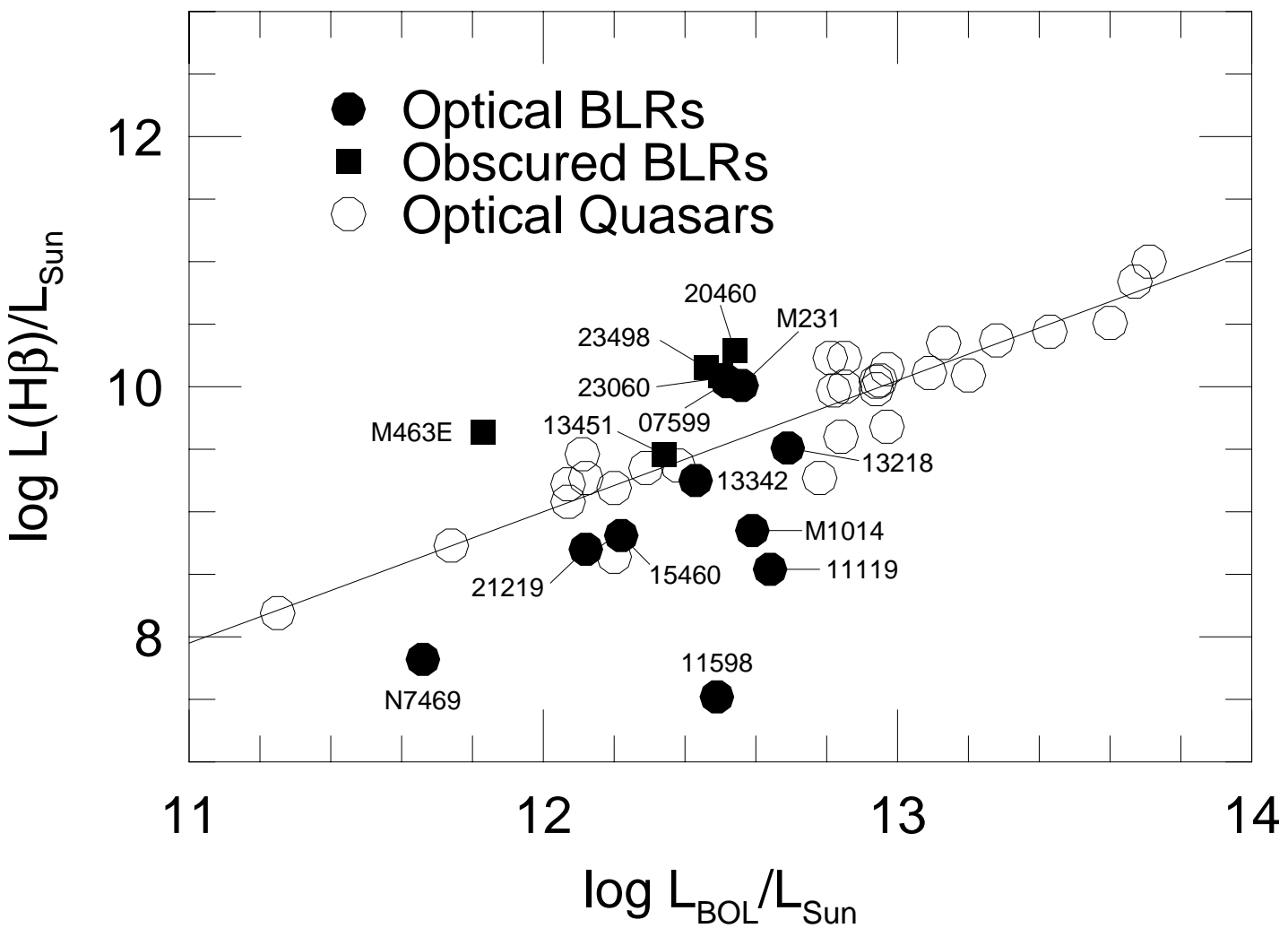


Fig. 16.—

TABLE 1  
JOURNAL OF OBSERVATIONS

Obs. Date	Grating (1/mm)	Spectral Range (Å)	Resolution (Å)	Seeing (")	CCD
1994 Feb 2-5	300	4550 – 8940	8.3	1.5–3.0	Ford F3KA 3072x512
1995 Mar 26-29	300	4720 – 8990	8.3	2.1–3.0	Ford F3KC 3072x512
1995 Oct 24-28	300	4080 – 8970	8.3	1.0–1.5	Ford F3KC 3072x512

TABLE 2  
SPECTROSCOPIC 1-JY SURVEY

IRAS FSC (1)	$z$ (2)	$\log\left(\frac{L_{\text{IR}}}{L_{\odot}}\right)$ (3)	Type (4)
00091-0738	0.118	12.19	H (1)
00188-0856	0.128	12.33	L (1)
00397-1312	0.261	12.90	H (1)
00456-2904	0.110	12.12	H (1)
00482-2721	0.129	12.00	L (1)
01004-2237	0.118	12.24	H (1)
01166-0844	0.118	12.03	H (1)
01199-2307	0.156	12.26	H (1)
01298-0744	0.136	12.27	H (1)
01355-1814	0.192	12.39	H (1)
01494-1845	0.158	12.23	...
01569-2939	0.141	12.15	H (1)
01572+0009	0.163	12.53	S1 (1,7)
02021-2103	0.116	12.01	...
02411+0353	0.144	12.19	H (1)
02480-3745	0.165	12.23	...
03209-0806	0.166	12.19	H (1)
03250+1606	0.129	12.06	L (1)
Z03521+002	0.152	12.45	L (1)
04074-2801	0.153	12.14	L (1)
04103-2838	0.118	12.15	L (1)
04313-1649	0.268	12.55	...
05020-2941	0.154	12.28	L (1)
05024-1941	0.192	12.43	S2 (1)
05156-3024	0.171	12.20	S2 (1)
05189-2524	0.042	12.07	S2 (6)
07599+6508	0.149	12.46	S1 (4,6,7)
08201+2801	0.168	12.23	H (4)
08474+1813	0.145	12.13	...
08559+1053	0.149	12.16	S2 (1, 4)
08572+3915	0.058	12.11	L (4,6)
08591+5248	0.158	12.14	...
09039+0503	0.125	12.07	L (1)
09116+0334	0.146	12.11	L (1)
09463+8141	0.156	12.29	L (1)
09539+0857	0.129	12.03	L (1)
10035+2740	0.165	12.22	...
10091+4704	0.246	12.67	L (4)
10190+1322	0.077	12.00	H (1)
10378+1108	0.136	12.26	L (1)
10485-1447	0.133	12.17	L (1)
10494+4424	0.092	12.13	L (4)
10594+3818	0.158	12.24	H (1)
11028+3130	0.199	12.32	L (4)
11095-0238	0.106	12.20	L (1)
11119+3257	0.189	12.58	S1 (4)
11130-2659	0.136	12.05	L (1)
11180+1623	0.166	12.24	L (1)
11223-1244	0.199	12.59	S2 (4)
11387+4116	0.149	12.18	H (1)
11506+1331	0.127	12.28	H (4)
11582+3020	0.223	12.56	L (4)
Z11598-0112	0.151	12.43	S1 (1)
12018+1941	0.168	12.44	...
12032+1707	0.217	12.57	L (1)
12072-0444	0.129	12.35	S2 (4,6)
12112+0305	0.073	12.28	L (4)
12127-1412	0.133	12.10	L (1)
12265+0219	0.159	12.73	S1 (7)
12359-0725	0.138	12.11	L (1)

TABLE 2—*Continued*

IRAS FSC (1)	$z$ (2)	$\log\left(\frac{L_{\text{IR}}}{L_{\odot}}\right)$ (3)	Type (4)
12447+3721	0.158	12.06	H (1)
12540+5708	0.042	12.50	S1 (4,6,7)
13106-0922	0.174	12.32	L (1)
13218+0552	0.205	12.63	S1 (4,5)
13305-1739	0.148	12.21	S2 (1,2)
13335-2621	0.125	12.06	L (1)
13342+3932	0.179	12.37	S1 (4)
13428+5608	0.037	12.10	S2 (4,6) <sup>a</sup>
13443+0802	0.135	12.15	S2 (1)
13451+1232	0.122	12.28	S2 (4)
13454-2956	0.129	12.21	S2 (4)
13469+5833	0.158	12.15	H (1)
13509+0442	0.136	12.27	H (1)
13539+2920	0.108	12.00	H (1)
14053-1958	0.161	12.12	S2 (1)
14060+2919	0.117	12.03	H (4)
14070+0525	0.265	12.76	S2 (4)
14121-0126	0.151	12.23	L (1)
14197+0813	0.131	12.00	...
14202+2615	0.159	12.39	H (4)
14252-1550	0.149	12.15	L (1)
14348-1447	0.083	12.28	L (4,6)
14394+5332	0.105	12.04	S2 (4)
14485-2434	0.148	12.04	...
15001+1433	0.162	12.38	S2 (4)
15043+5754	0.151	12.05	H (1)
15130-1958	0.109	12.09	S2 (4)
15206+3342	0.125	12.18	H (4)
15225+2350	0.139	12.10	H (1)
15327+2340	0.018	12.17	L (4,6) <sup>b</sup>
15462-0450	0.100	12.16	S1 (4)
16090-0139	0.134	12.49	L (4)
16156+0146	0.132	12.04	S2 (1)
16300+1558	0.242	12.63	L (4)
16333+4630	0.191	12.35	L (4)
16468+5200	0.150	12.02	L (4)
16474+3430	0.111	12.11	H (4)
16487+5447	0.104	12.12	L (4)
17028+5817	0.106	12.10	L (4)
17044+6720	0.135	12.13	L (4)
17068+4027	0.179	12.30	H (4)
17179+5444	0.147	12.20	S2 (1)
20414-1651	0.086	12.14	H (4)
21208-0519	0.130	12.01	H (1)
21219-1757	0.113	12.06	S1 (1)
21329-2346	0.125	12.09	L (4)
21477+0502	0.171	12.24	L (1)
22088-1831	0.170	12.31	H (1)
22206-2715	0.132	12.19	H (1)
22491-1808	0.076	12.09	H (6)
22541+0833	0.166	12.23	S2 (1)
23060+0505	0.173	12.44	S2 (1)
23129+2548	0.179	12.38	L (1)
23233+2817	0.114	12.00	S2 (1)
23234+0946	0.128	12.05	L (1)
23327+2913	0.107	12.06	L (1)
23389+0300	0.145	12.09	S2 (1)
23498+2423	0.212	12.40	S2 (1)

Column (1) – Target name. FSC is the prefix given to the name of all sources in the *IRAS* Faint Source Catalog (c.f. Moshir et al. 1992). The prefix ‘Z’ is used for objects that are not in the FSC – these objects are contained in the Faint Source Reject File (see Moshir et al. 1992).

Column (2) – Optical redshift from Kim & Sanders (1998).

Column (3) – Infrared luminosity (see text).

Column (4) – Spectral type: HII = H II galaxy, L = LINER, S2 = Seyfert 2, S1 = Seyfert 1. Numbers in parentheses are references.

<sup>a</sup>This object was classified as a LINER by Veilleux et al. (1995). The reclassification of this object is due to a slight change in the [O III]  $\lambda$ 5007/H $\beta$  ratio which may be attributable to differences in the extraction apertures between the two sets of data.

<sup>b</sup>This object was classified as a Seyfert 2 by Veilleux et al. (1995). The present classification is considered more reliable because the data are of better quality and are less affected by centering errors.

REFERENCES.—For spectral type: (1) This work, (2) Allen et al. 1991, (3) Hill et al. 1988, (4) Kim, Veilleux, & Sanders 1998, (5) Low et al. 1988, (6) Veilleux et al. 1995, (7) Véron-Cetty & Véron 1989



TABLE 3  
EMISSION-LINE FLUXES, LUMINOSITIES, AND ELECTRON DENSITIES

Name IRAS FSC (1)	$F_{H\alpha}$ (2)	$EW_{H\alpha}$ (3)	$L_{H\alpha}$ log (4)	H $\beta$ 4861 (5)	[O III] 5007 (6)	[O I] 6300 (7)	[N II] 6583 (8)	[S II] 6716 (9)	[S II] 6731 (10)	$n_e$ cm $^{-3}$ (11)
00091–0738	0.20	29	8.21	0.12	0.08	0.03	0.48	0.24	0.19	180
00188–0856	0.35	23	9.05	0.07	0.20	0.12	1.35	3.59s	...	...
00397–1312	1.30	213	9.61	0.14	0.18	0.05	0.47	0.31s	...	...
00456–2904	2.04	113	8.91	0.16	0.10	0.04	0.50	0.19	0.14	100
00482–2721	0.27	47	8.50	0.11	0.21	0.18	0.65	0.20:s	...	...
01004–2237	1.78	156	8.95	0.15	0.74	0.06	0.16	0.07	0.04	...
01166–0844	0.15	30	7.43	0.23:	0.05:	...	0.48	0.14	0.10	110
01199–2307	0.41:	67	8.58:	0.15	0.16	0.13	0.30	0.20	0.16	180
01298–0744	0.16	37	8.03	0.15	0.17	0.14	0.42	0.39s	...	...
01355–1814	0.23	107	8.42	0.16	0.16	0.05	0.46	0.29s	...	...
01569–2939	1.46	246	10.00	0.06	0.13	0.09	0.50	0.14	0.18	1310
01572+0009	...	...	...	...	...	...	...	...	...	...
02411+0353:main	1.99	287	9.16	0.16	0.16	0.03	0.43	0.13	0.10	180
02411+0353:E	0.42	55	8.24	0.20	0.16	0.06	0.42	0.19	0.15	110
02411+0353:W	0.76	128	8.88	0.14	0.10	0.02	0.39	0.13	0.13	450
03209–0806	0.56	53	9.28	0.09	0.08	0.04	0.66	0.38s	...	...
03250+1606†	0.44	39	9.53	0.05	0.09	0.09	0.72	0.47s	...	...
Z03521+0028	0.08	42	9.54	0.03:	0.06:	0.07:	0.83:	0.56:s	...	...
04074–2801	0.07	10	8.10	0.11	0.28	0.23	0.76:	1.07s	...	...
04103–2838	1.42	121	9.28	0.09	0.32	0.08	0.60	0.17	0.13	180
05020–2941	0.69	118	8.66	0.16	0.22	0.07	0.41	0.23	0.17	120
05024–1941	0.21:	24	9.78:	0.04:	0.42	0.06:	1.78:	0.21	0.15	<100
05156–3024	0.82	117	9.11	0.12	1.14	0.12	1.40	0.52s	...	...
05189–2524	2.90	34	9.36	0.12:	5.28	0.17	3.19	0.46	0.18	<100
07599+6508	37::	162::	...	...	...	...	...	...	...	...
08201+2801	0.36	82	8.26	0.21	0.13	0.05	0.47	0.19	0.10	...
08559+1053†	0.92	78	8.93	0.14	0.86	0.08	0.71	0.32	0.01	...
08572+3915:NW	0.89	72	9.13	0.05	0.13	0.05	0.43	0.26	0.23	350
08572+3915:SE	0.40	41	8.70	...	0.05	0.13	0.02	0.38	0.15	...
09039+0503†	0.65	68	8.48	0.16	0.14	0.12	0.80	0.25	0.33	1570:
09116+0334†	0.61	28	9.69	0.05	0.10	0.09	0.95	0.22	0.18	240
09463+8141	0.12:	25	9.26:	0.04:	0.13:	0.10:	0.60:	0.78:s	...	...
09539+0857†	0.25	42	8.55	0.10	0.24	0.19	0.67	0.61s	...	...
10091+4704	0.18	29	9.19	0.08	0.09	0.09	0.80	0.70s	...	...
10190+1322	1.07	45	8.67	0.11	0.03	0.05	0.51	0.24s	...	...
10378+1108†	0.75	8	7.82	0.15	0.20	0.14	1.00	0.55:s	...	...
10485–1447	0.09	23	8.68	0.06:	0.13:	0.15	0.69	0.28:s	...	...
10494+4424	0.31	37	8.18	0.11	0.15	0.13	0.60	0.23	0.22	550
10594+3818	1.25:	112	8.96:	0.17	0.10	0.05	0.56:	0.17	0.13	160
11028+3130	0.03	8	6.96	0.29	0.12	0.18	1.15	0.68s	...	...

TABLE 3—*Continued*

Name IRAS FSC (1)	$F_{H\alpha}$ (2)	$EW_{H\alpha}$ (3)	$L_{H\alpha}$ log (4)	$H\beta$ 4861 (5)	[O III] 5007 (6)	[O I] 6300 (7)	[N II] 6583 (8)	[S II] 6716 (9)	[S II] 6731 (10)	$n_e$ cm <sup>-3</sup> (11)
11095-0238†	0.64	105	8.22	0.17	0.21	0.13	0.58	0.27	0.21	140
11119+3257	117::	222::	...	...	...	...	...	...	...	...
11130-2659	0.14	22	8.35	0.10:	0.16	0.12:	0.62	0.43:s	...	...
11180+1623	0.29:	59	8.87:	0.10	0.12	0.09	0.52:	0.20:	0.22:	820:
11223-1244	0.20	39	10.33	0.02:	0.32	0.08	1.05	0.37	0.19	...
11387+4116†	0.31	33	9.00	0.08	0.13	0.04	0.80	0.20	0.17	320
11506+1331	0.47	88	8.73	0.10	0.13	0.10	0.42	0.19	0.16	230
11582+3020	0.25	50	8.59	0.16	0.15	0.14	0.79	0.19	0.21	820
Z11598-0112	1.53:	85	8.49:	0.29	0.20	0.03	0.33:	0.07	0.04	...
12032+1707	1.65	211	9.61	0.13	0.15	0.20	0.93	0.54s	...	...
12072-0444	1.70	174	9.90	0.06	0.45	0.09	0.71	0.32	0.20	...
12112+0305	0.80	65	8.27	0.13	0.27	0.12	0.64	0.54s	...	...
12127-1412	0.28	48	9.14	0.06:	0.08	0.05	0.91	0.19:s	...	...
12265+0219	...	...	...	...	...	...	...	...	...	...
12359-0725:N	0.25	77	8.05	0.17	0.34	0.12	0.60	0.21	0.21	570
12359-0725:S	0.39	122	8.06	0.22	0.37	0.03	0.23	0.17s	...	...
12447+3721	2.06:	436	9.04:	0.19	0.47	0.04	0.26:	0.13	0.11	260
12540+5708	135::	168::	...	...	...	...	...	...	...	...
13106-0922	0.33	94	8.52	0.15	0.27	0.13	0.49	0.21	0.25	1090
13218+0552	1.98	390	9.52	0.14	0.29	0.04	0.25	0.06	0.04	...
13305-1739	9.55:	349	10.25:	0.10	1.10	0.07	0.34:	0.21s	...	...
13335-2612	0.56	92	8.77	0.11	0.22	0.07	0.42	0.23	0.19	220
13342+3932	4.12	300	10.45	0.07	0.28	0.02	0.53	0.03	0.03	850
13428+5608	8.21	96	8.97	0.10	0.36	0.13	1.01	0.31	0.27	280
13443+0802:NE	1.01	53	9.20	0.10	0.05	0.05	0.60	0.38:s	...	...
13443+0802:SW	0.36	66	9.13	0.07	1.22	0.17	1.06	0.61:s	...	...
13451+1232	2.80	247	9.62	0.09	0.83	0.23	0.75	0.22	0.21	450
13454-2956	0.12	25	8.58	0.07	0.40	0.06	1.04	0.44s	...	...
13469+5833	0.28:	37	8.89:	0.09	0.06	0.02	0.57:	0.19	0.18	450
13509+0442	1.14	164	9.24	0.11	0.09	0.05	0.44	0.36:s	...	...
13539+2920	1.02	92	9.34	0.07	0.09	0.06	0.51	0.21	0.18	280
14053-1958	0.11:	24	7.51:	0.24:	0.94	0.28	1.19:	0.88s	...	...
14060+2919	3.03	194	9.23	0.14	0.11	0.04	0.46	0.17	0.15	370
14070+0525	0.11	26	9.76	0.04	0.19	0.13	0.82	0.36	0.36	560
14121-0126	0.47	67	9.23	0.08	0.13	0.13	1.13	0.30	0.21	<100
14202+2615	1.20	170	8.99	0.16	0.13	0.04	0.46	0.17	0.13	170
14252-1550	0.19	38	9.01	0.06:	0.10:	0.06:	0.57	0.34s	...	...
14348-1447:SW	1.16	90	8.73	0.11	0.15	0.11	0.65	0.26	0.20	140
14348-1447:NE	0.49	46	8.40	0.10:	0.15	0.15	0.67	0.34	0.24	<100
14394+5332	4.49	158	9.36	0.13	0.43	0.19	0.94	0.43	0.19	...

TABLE 3—*Continued*

Name IRAS FSC (1)	$F_{H\alpha}$ (2)	$EW_{H\alpha}$ (3)	$L_{H\alpha}$ log (4)	H $\beta$ 4861 (5)	[O III] 5007 (6)	[O I] 6300 (7)	[N II] 6583 (8)	[S II] 6716 (9)	[S II] 6731 (10)	$n_e$ cm $^{-3}$ (11)
15001+1433	0.64	69	8.89	0.13	0.48	0.06	0.65	0.22	0.23	640
15043+5754	0.48	73	8.75	0.13	0.12	0.04	0.41	0.23	0.11	...
15130-1958	1.05:	98	10.05:	0.04:	0.88	0.07	0.84:	0.28s	...	...
15206+3342	7.67	397	9.55	0.17	0.52	0.03	0.22	0.08	0.06	210
15225+2350	0.66	81	9.44	0.07	0.19	0.05	0.48	0.14:	0.18:	1260:
15327+2340	1.09	15	7.29	0.11	0.13	0.18	2.39	1.06s	...	...
15462-0450	5.58:	167	9.08:	0.18	0.18	0.01	0.38:	0.07s	...	...
16090-0139	1.31	128	9.66	0.07	0.08	0.08	0.77	0.24	0.16	...
16156+0146	0.78	211	8.57	0.16	1.53	0.15	0.45	0.35:s	...	...
16300+1558	0.22	40	8.89	0.12	0.15	0.11	0.60	0.32	0.19	...
16333+4630	0.49	99	8.98	0.12	0.20	0.06	0.58	0.24	0.17	<100
16468+5200:W	0.15	46	8.28	0.12	0.08	0.02	0.64	0.32	0.35	820
16468+5200:E	0.09	30	8.40	0.09	0.10	0.06:	0.69	0.43	0.38	370
16474+3430	1.28	87	8.30	0.24	0.26	0.06	0.48	0.16	0.15	510
16487+5447	2.92	184	8.71	0.20	0.32	0.07	0.58	0.21	0.15	<100
17028+5817:W	0.44	71	8.90	0.07	0.11	0.11	0.57	0.20	0.22	740
17028+5817:E	0.79	135	8.39	0.18	0.20	0.02	0.28	0.18	0.13	<100
17044+6720	0.57	98	8.63	0.14	0.37	0.10	0.62	0.23	0.13	...
17068+4027	0.91	227	9.67	0.08	0.17	0.03	0.34	0.22	0.15	...
17179+5444	0.69	55	9.12	0.10	0.97	0.12	1.19	0.53s	...	...
20414-1651	0.37	47	8.34	0.11	0.08	0.11	0.54	0.18	0.14	180
21208-0519:N	0.48	89	8.54	0.13	0.10	0.04	0.47	0.29:s	...	...
21208-0519:S	0.12	...	8.47	0.12	0.22	0.23	0.43	0.46:s	...	...
21219-1757	...	...	...	...	...	...	...	...	...	...
21329-2346	0.50	78	8.30	0.17	0.16	0.10	0.61	0.45s	...	...
21477+0502	0.14	52	7.99	0.17	0.24	0.11	0.57	0.34s	...	...
22088-1831	0.18	34	7.98	0.21	0.09:	0.04	0.48	0.56:s	...	...
22206-2715	0.64	60	8.67	0.14	0.14	0.08	0.49	0.08	0.11:	2170:
22491-1808	2.30	77	8.71	0.37	0.25	0.12	0.99	0.34	0.23	<100
22541+0833:NW	0.14	28	7.66	0.24	0.32	0.04	0.66	0.41:s	...	...
22541+0833:SE	0.13:	6	9.91:	0.26:	0.33:	0.04:	0.68:	0.36:s	...	...
23060+0505	2.75	202	10.00	0.09	0.77	0.03	0.27	0.19s	...	...
23129+2548	0.11	26	8.71	0.08	0.11	0.08	0.64	0.33s	...	...
23233+2817	0.94	54	8.77	0.13	1.60	0.07	1.67	0.20	0.03	...
23234+0946	1.10	217	8.83	0.14	0.17	0.11	0.81	0.48:s	...	...
23327+2913	0.23	39	9.16	0.04:	0.07:	0.08:	0.91	0.24	0.16	...
23389+0300	0.61:	288	8.94:	0.11	0.48	0.78	2.13:	0.84s	...	...
23498+2423	0.63	89	9.10	0.14	1.50	0.05	0.62	0.18	0.13	<100

Column (1) – Target name. († = non-photometric data)

Column (2) – Absolute flux of H $\alpha$  in units of  $10^{-14}$  erg s $^{-1}$  cm $^{-2}$ .

Column (3) – Equivalent widths of the H $\alpha$  emission line in  $\text{\AA}$  derived in the rest frames of the objects.

Column (4) – Logarithms of the dereddened H $\alpha$  luminosities in units of the bolometric solar luminosity ( $3.83 \times 10^{33}$  erg s $^{-1}$ ).

Column (5) – Flux of H $\beta$  relative to H $\alpha$ . This is the weighted average of the values obtained from the standard plotting package of IRAF ('splot') and the fitting procedures, with weights estimated from the relative uncertainties in the two types of measurements.

Column (6) – Flux of [O III]  $\lambda$ 5007 relative to H $\alpha$ .

Column (7) – Flux of [O I]  $\lambda$ 6300 relative to H $\alpha$ .

Column (8) – Flux of [N II]  $\lambda$ 6583 relative to H $\alpha$ .

Column (9) – Flux of [S II]  $\lambda$ 6716 relative to H $\alpha$ . Entry followed by the letter “s” represents the sum

TABLE 4  
 ABSORPTION PROPERTIES, LINE WIDTHS, AND CONTINUUM LEVELS

Name IRAS FSC (1)	$EW(\text{\AA})$			$FWHM$ [O III] (5)	C4861 (6)	C6563 (7)
	H $\beta$ (2)	Mg Ib (3)	Na ID (4)			
00091-0738	2.8	...	2.8	...	0.65	0.69
00188-0856	5.5	...	5.3	...	1.45	1.46
00397-1312	2.8:	...	3.6	440	0.68	0.61
00456-2904	...	...	6.1	340	1.93	1.80
00482-2721	...	...	...	...	0.58	0.56
01004-2237	...	...	...	...	1.41	1.14
01166-0844	4.2	3.4	...	...	0.61	0.47
01199-2307	...	...	1.5	30:	0.68	0.61
01298-0744	3.1	...	4.2	...	0.38	0.42
01355-1814	...	...	...	...	0.30	0.22
01569-2939	...	...	2.1	410	0.61	0.59
01572+0009	...	...	...	810	9.49	6.15
02411+0353:main	...	1.5	5.4	20:	0.61	0.69
02411+0353:E	6.1	...	2.0	...	0.78	0.76
02411+0353:W	2.5	...	1.3	150	0.59	0.59
03209-0806	1.1:	1.8	6.6	390	1.08	1.05
03250+1606 †	2.5	1.0:	6.0	320:	0.87	1.12
Z03521+0028	...	...	...	...	0.13	0.19
04074-2801	4.7	...	3.2	...	0.67	0.69
04103-2838	...	2.1	4.9	390	1.01	1.17
05020-2941	...	...	...	...	0.68	0.58
05024-1941	...	...	8.2	1380:	0.78	0.88
05156-3024	...	...	2.5	950	0.59	0.70
05189-2524	3.1	0.9	4.4	540	10.0	8.60
07599+6508	...	...	...	...	...	...
08201+2801	...	1.3	4.6	510	0.50	0.44
08559+1053 †	...	1.8	3.2	690	1.23	1.18
08572+3915:NW	...	0.7	3.5	70:	1.07	1.23
08572+3915:SE	...	0.2	2.7	...	0.77	0.99
09039+0503 †	...	1.2:	3.9	470	0.96	0.96
09116+0334 †	4.4	0.8:	3.7	...	2.49	2.17
09463+8141	...	...	...	...	0.47	0.50
09539+0857 †	...	...	3.2	130	0.64	0.58
10091+4704	0.8	2.2	3.2	360	0.57	0.62
10190+1322	2.8	...	4.9	...	1.85	2.34
10378+1108 †	...	...	3.4	490	1.45	1.21
10485-1447	...	...	6.1	...	0.33	0.38
10494+4424	8.2	0.1	4.1	...	0.52	0.83
10594+3818	3.7	...	2.9	230	1.32	1.11
11028+3130	5.6	1.5	2.7	...	0.36	0.31

TABLE 4—*Continued*

Name IRAS FSC (1)	$EW(\text{\AA})$			$FWHM$ [O III] (5)	C4861 (6)	C6563 (7)
	H $\beta$ (2)	Mg Ib (3)	Na ID (4)			
11095–0238 †	...	...	...	320	0.77	0.61
11119+3257	...	...	11.2	1420	...	...
11130–2659	4.2	1.1:	2.1:	...	0.63	0.61
11180+1623	6.1	...	4.5	210	0.47	0.48
11223–1244	2.8	2.3	6.9	960	0.36	0.50
11387+4116 †	...	...	8.2	...	0.82	0.94
11506+1331	1.0	0.8	4.9	80:	0.44	0.53
11582+3020	0.6	2.4	3.6	250	0.58	0.49
Z11598–0112	...	...	...	350	2.82	1.79
12032+1707	...	...	2.7	580	0.74	0.78
12072–0444	0.5	0.3	2.1	500	0.81	0.97
12112+0305	1.2	1.5	4.0	...	1.26	1.23
12127–1412	...	...	4.6	...	0.53	0.57
12265+0219	...	...	...	...	...	...
12359–0725:N	7.2	...	5.6	420	0.37	0.32
12359–0725:S	...	...	...	90:	0.38	0.32
12447+3721	...	...	2.1	190	0.57	0.47
12540+5708	...	...	...	...	...	...
13106–0922	...	3.1	5.7	160	0.37	0.34
13218+0552	...	2.4	0.8	1440	0.59	0.51
13305–1739	...	0.9	0.8:	1200	2.87	2.73
13335–2612	1.9:	1.5:	4.1	140	0.58	0.60
13342+3932	...	0.8	2.4	420	1.87	1.37
13428+5608	0.2	0.7	4.9	480	7.76	8.55
13443+0802:NE	2.2	2.2	6.2	500	1.56	1.89
13443+0802:SW	...	3.3	3.6	410	0.39	0.54
13451+1232	0.2	1.5	0.5	1250	0.80	1.13
13454–2956	...	0.2	1.9	70:	0.47	0.46
13469+5833	1.8:	2.1	3.7	...	0.61	0.74
13509+0442	...	...	3.6	...	0.65	0.69
13539+2920	...	...	5.8	440	0.90	1.11
14053–1958	3.3	...	...	420	0.34	0.43
14060+2919	0.7	1.1	2.8	200	1.56	1.56
14070+0525	0.7	1.5	4.6	...	0.34	0.42
14121–0126	4.6	...	6.0	590:	0.60	0.70
14202+2615	0.3	1.4	3.5	160	0.77	0.71
14252–1550	...	...	5.7	...	0.43	0.49
14348–1447:SW	3.4	0.6	4.8	440	1.00	1.28
14348–1447:NE	3.7	0.4	3.9	100	0.95	1.08
14394+5332	0.4	0.2	3.9	1870	2.41	2.83

TABLE 4—*Continued*

Name IRAS FSC (1)	$EW(\text{\AA})$			$FWHM$ [O III] (5)	C4861 (6)	C6563 (7)
	$H\beta$ (2)	Mg Ib (3)	NaID (4)			
15001+1433	0.6	1.1	4.2	280	0.96	0.91
15043+5754	...	...	1.6:	360	0.64	0.65
15130-1958	0.2	0.2	3.5	1100	0.92	1.07
15206+3342	0.1	0.2	1.9	60:	2.41	1.93
15225+2350	3.4	...	5.1	...	0.64	0.80
15327+2340	2.6	2.7	5.8	...	4.50	6.93
15462-0450	...	0.3	0.2	1560	3.24	3.33
16090-0139	0.5	1.8	4.4	150	0.79	1.02
16156+0146	...	...	...	590	0.38	0.37
16300+1558	2.1	1.0	5.4	120	0.56	0.54
16333+4630	0.6	0.3	3.4	450	0.45	0.49
16468+5200:W	...	...	4.3	...	0.33	0.32
16468+5200:E	...	...	...	...	0.28	0.31
16474+3430	2.2	0.4	1.6	...	1.92	1.47
16487+5447	0.1	1.4	1.2	340	2.16	1.58
17028+5817:W	0.9	1.5	5.9	80:	0.46	0.62
17028+5817:E	0.9	2.2	2.5	120	0.61	0.59
17044+6720	0.5	0.9	0.8	280	0.61	0.58
17068+4027	0.9	1.7	3.9	440	0.35	0.40
17179+5444	...	...	2.3	770	1.29	1.25
20414-1651	1.1	0.4	3.6	...	0.57	0.77
21208-0519:N	...	...	...	130	0.53	0.53
21208-0519:S	...	...	...	...	0.53	0.50
21219-1757	...	...	...	1120	14.20	9.55
21329-2346	3.1	2.2	2.9	290	0.87	0.63
21477+0502	6.0	...	...	180	0.29	0.27
22088-1831	2.8:	2.3:	2.7	...	0.53	0.52
22206-2715	1.8	...	1.5	150	1.20	1.06
22491-1808	2.2	0.9	1.8	...	3.70	3.00
22541+0833:NW	3.4	...	...	...	0.45	0.51
22541+0833:SE	...	...	9.6	160	1.65	1.95
23060+0505	...	...	...	570	0.95	1.36
23129+2548	4.7	...	3.7	...	0.45	0.43
23233+2817	...	1.6	1.1	610	1.59	1.74
23234+0946	...	...	...	450	0.60	0.51
23327+2913	...	...	4.0	...	0.37	0.59
23389+0300	...	...	2.6	820	0.37	0.21
23498+2423	...	...	1.2	420	0.62	0.70

Column (1) – Target name. († = non-photometric data)

Column (2) – Equivalent widths of the  $H\beta$  absorption feature in  $\text{\AA}$  derived from the fitting method and in the rest frames of the objects. The typical uncertainties on these measurements are about 50 %, and for some of the objects with strong  $H\beta$  emission line they are > 50 % (values flagged with a colon).

Column (3) – Equivalent widths of the Mg Ib  $\lambda 5176$  absorption feature in  $\text{\AA}$  derived in the rest frames of the objects. The typical uncertainties on these measurements are about 20 – 50 %, and for some of the objects they are > 50 % (values flagged with a colon).

Column (4) – Equivalent widths of the  $H\beta$  absorption feature in  $\text{\AA}$  derived in the rest frames of the objects. The typical uncertainties on these measurements are about 20 – 50 %, and for some of the objects they are > 50 % (values flagged with a colon).

Column (5) – Line widths of [O III]  $\lambda 5007$  in  $\text{km s}^{-1}$  after correction for the finite instrument resolution of the data using the quadrature method. Uncertainties on these measurements are about  $\pm 100 - 200 \text{ km s}^{-1}$ . Corrected line widths below  $100 \text{ km s}^{-1}$  are flagged with a colon in Table 4 to emphasize the large uncertainties on these measurements.

TABLE 5  
OBSERVED AND DEREDDENED LINE RATIOS AND SPECTRAL CLASSIFICATION

Name IRAS FSC (1)	$\frac{H\alpha}{H\beta}$ log (2)	$E(B - V)$ (3)	$\frac{[O III]}{H\beta}$ log (4)	$\frac{[N II]}{H\alpha}$ log (5)	$\frac{[S II]}{H\alpha}$ log (6)	$\frac{[O I]}{H\alpha}$ log (7)	Spectral Type			
							[N II] (8)	[S II] (9)	[O I] (10)	Adopt (11)
00091-0738	0.91 0.45	1.05	-0.21 -0.26	-0.32 -0.32	-0.37 -0.40	-1.54 -1.49	H	L	H	H:
00188-0856	1.17 0.49	1.56	0.47 0.39	0.13 0.12	-0.44 -0.49	-0.93 -0.85	L	L	L	L
00397-1312	0.86 0.45	0.93	0.09 0.04	-0.35 -0.36	-0.53 -0.56	-1.28 -1.23	H	H	H	H
00456-2904	0.80 0.45	0.81	-0.19 -0.23	-0.30 -0.30	-0.47 -0.50	-1.41 -1.37	H	H	H	H
00482-2721	0.97 0.49	1.11	0.29 0.24	-0.18 -0.19	-0.71: -0.74:	-0.74 -0.68	L	H	L	L:
01004-2237	0.82 0.45	0.84	0.69 0.65	-0.80 -0.80	-0.97 -1.00	-1.23 -1.18	H	H	S2	H:
01166-0844	0.63 0.45	0.41	-0.67: -0.69:	-0.32 -0.32	-0.61 -0.63	... ...	H	H	...	H:
01199-2307	0.83 0.45	0.86	0.02 -0.02	-0.53: -0.53:	-0.44: -0.46:	-0.87: -0.83:	H	H	L	H:
01298-0744	0.82 0.45	0.85	0.05 0.01	-0.38 -0.38	-0.40 -0.43	-0.85 -0.81	H	H	L	H:
01355-1814	0.78 0.45	0.76	0.00 -0.04	-0.34 -0.34	-0.54 -0.56	-1.29 -1.25	H	H	H	H
01569-2939	1.25 0.45	1.83	0.35 0.26	-0.30 -0.31	-0.50 -0.56	-1.04 -0.94	H	H	L	H:
01572+0009	... 0.45	...	0.11 ...	... ...	... ...	... ...	...	...	...	S1
02411+0353:main	0.80 0.45	0.79	-0.01 -0.05	-0.37 -0.37	-0.64 -0.67	-1.51 -1.47	H	H	H	H
02411+0353:E	0.69 0.45	0.55	-0.10 -0.13	-0.38 -0.38	-0.47 -0.48	-1.23 -1.20	H	H	H	H
02411+0353:W	0.86 0.45	0.93	-0.14 -0.19	-0.41 -0.41	-0.58 -0.61	-1.61 -1.57	H	H	H	H
03209-0806	1.05 0.45	1.37	-0.07 -0.14	-0.18 -0.18	-0.43 -0.47	-1.35: -1.28:	L	H	H	H:
03250+1606†	1.33 0.49	1.93	0.27 0.18	-0.14 -0.15	-0.33 -0.39	-1.07 -0.97	L	L	L	L
Z03521+0028	1.59 0.49	2.54	0.38: 0.26:	-0.08: -0.10:	-0.25: -0.33:	-1.16: -1.03:	L	L	L	L
04074-2801	0.98 0.49	1.12	0.43 0.38	-0.12: -0.12:	0.03 0.00	-0.64 -0.58	L	L	L	L
04103-2838	1.03 0.49	1.25	0.54 0.48	-0.22 -0.22	-0.52 -0.56	-1.07 -1.01	L	H	L	L:
05020-2941	0.79 0.49	0.69	0.13: 0.09:	-0.38: -0.39:	-0.40: -0.42:	-1.14: -1.10:	H	L	L	L:
05024-1941	1.41 0.49	2.13	1.04: 0.94:	0.25: 0.24:	-0.45: -0.51:	-1.25: -1.14:	S2	S2	S2	S2
05156-3024	0.91 0.49	0.97	0.97 0.92	0.15 0.14	-0.28: -0.31:	-0.91 -0.86	S2	S2	S2	S2

TABLE 5—*Continued*

Name IRAS FSC (1)	$\frac{H\alpha}{H\beta}$ log (2)	$E(B - V)$ (3)	$\frac{[O III]}{H\beta}$ log (4)	$\frac{[N II]}{H\alpha}$ log (5)	$\frac{[S II]}{H\alpha}$ log (6)	$\frac{[O I]}{H\alpha}$ log (7)	Spectral Type			
							[N II] (8)	[S II] (9)	[O I] (10)	Adopt (11)
05189–2524	1.37: 0.49	2.03:	1.63: 1.53:	0.04 0.03	–0.66 –0.72	–1.22 –1.12	S2	S2	S2	S2
07599+6508	... 0.49	...	...	...	...	...	...	...	...	S1
08201+2801	0.68 0.45	0.53	–0.19 –0.21	–0.32 –0.33	–0.54 –0.55	–1.32 –1.29	H	H	H	H
08559+1053 †	0.87 0.49	0.87	0.80 0.76	–0.15 –0.16	–0.49 –0.51	–1.09 –1.04	S2	S2	S2	S2
08572+3915:NW	1.33 0.49	1.94	0.46 0.36	–0.37 –0.38	–0.31 –0.37	–1.30 –1.20	H	L	L	L:
08572+3915:SE	1.29 0.49	1.85	0.42 0.33	0.00 –0.01	–0.28 –0.34	–1.78 –1.69	L	L	H	L:
09039+0503 †	0.81 0.49	0.73	–0.05 –0.09	–0.10 –0.10	–0.24 –0.26	–0.91 –0.87	L	L	L	L
09116+0334 †	1.28 0.49	1.83	0.26: 0.18:	–0.02 –0.03	–0.40 –0.46	–1.07 –0.97	L	H	L	L:
09463+8141	1.37 0.49	2.03	0.48: 0.38:	–0.22: –0.23:	–0.11: –0.17:	–1.01: –0.91:	L	L	L	L
09539+0857 †	1.01 0.49	1.19	0.38 0.33	–0.18 –0.18	–0.21 –0.25	–0.72 –0.66	L	L	L	L
10091+4704	1.08 0.49	1.36	0.05 –0.02	–0.10 –0.10	–0.16 –0.20	–1.06 –0.99	L	H	L	L:
10190+1322	0.95 0.45	1.15	–0.64 –0.70	–0.29 –0.30	–0.61 –0.65	–1.34 –1.28	H	H	H	H
10378+1108 †	0.83 0.49	0.78	0.13 0.09	0.00 –0.01	–0.26: –0.28:	–0.85 –0.81	L	L	L	L
10485–1447	1.24 0.49	1.74	0.35: 0.27:	–0.16: –0.17:	–0.56: –0.61:	–0.83: –0.74:	L	H	L	L:
10494+4424	0.94 0.49	1.04	0.12 0.07	–0.22 –0.23	–0.35 –0.38	–0.90 –0.85	L	L	L	L
10594+3818	0.78 0.45	0.75	–0.24 –0.28	–0.25: –0.25:	–0.53: –0.55:	–1.26: –1.23:	H	H	H	H
11028+3130	0.53 0.49	0.10	–0.37 –0.38	0.06 0.06	–0.17 –0.17	–0.74 –0.74	L	L	L	L
11095–0238 †	0.76 0.49	0.62	0.09 0.06	–0.24 –0.24	–0.32 –0.34	–0.87 –0.84	L	L	L	L
11119+3257	... 0.49	...	–0.04 ...	... ...	... ...	... ...	...	...	...	S1
11130–2659	1.01 0.49	1.21	0.23: 0.17:	–0.20 –0.21	–0.36: –0.40:	–0.93: –0.87:	L	L	L	L
11180+1623	1.01 0.49	1.21	0.09 0.03	–0.28: –0.29:	–0.38: –0.42:	–1.06: –1.00:	H	L	L	L:
11223–1244	1.65 0.49	2.68	1.16 1.03	0.02 0.01	–0.25 –0.34	–1.10 –0.96	S2	S2	S2	S2
11387+4116 †	1.08 0.45	1.45	0.20 0.13	–0.09 –0.10	–0.43 –0.47	–1.44 –1.37	L	H	H	H:



TABLE 5—*Continued*

Name IRAS FSC (1)	$\frac{H\alpha}{H\beta}$ log (2)	$E(B - V)$ (3)	$\frac{[O III]}{H\beta}$ log (4)	$\frac{[N II]}{H\alpha}$ log (5)	$\frac{[S II]}{H\alpha}$ log (6)	$\frac{[O I]}{H\alpha}$ log (7)	Spectral Type			
							[N II] (8)	[S II] (9)	[O I] (10)	Adopt (11)
11506+1331	0.98 0.45	1.13	0.08 0.02	-0.37 -0.38	-0.46 -0.50	-0.98 -0.92	H	H	L	H:
11582+3020	0.82 0.49	0.76	0.04 0.00	-0.13 -0.14	-0.38 -0.40	-0.89 -0.85	L	L	L	L
Z11598-0112	0.54 0.45	0.19	-0.16 -0.17	-0.48: -0.48:	-0.99: -1.00:	-1.52: -1.51:	...	...	...	S1
12032+1707	0.90 0.49	0.94	0.07 0.03	-0.03 -0.03	-0.27 -0.30	-0.69 -0.64	L	L	L	L
12072-0444	1.23 0.49	1.71	0.88 0.80	-0.15 -0.15	-0.29 -0.34	-1.07 -0.98	S2	S2	S2	S2
12112+0305	0.89 0.49	0.92	0.32 0.28	-0.19 -0.20	-0.27 -0.29	-0.93 -0.89	L	L	L	L
12127-1412	1.23 0.49	1.71	0.13: 0.05:	-0.04: -0.05:	-0.73: -0.78:	-1.27: -1.19:	L	H	L	L:
12265+0219	... 0.49	...	... ...	... ...	... ...	... ...	...	...	...	S1
12359-0725:N	0.76 0.49	0.63	0.29 0.26	-0.22 -0.23	-0.38 -0.40	-0.91 -0.87	L	L	L	L
12359-0725:S	0.66 0.45	0.47	0.22 0.20	-0.64 -0.64	-0.76 -0.78	-1.51 -1.48	H	H	H	H
12447+3721	0.72 0.45	0.61	0.39 0.36	-0.59: -0.59:	-0.64: -0.65:	-1.44: -1.41:	H	H	H	H
12540+5708	... 0.49	...	... ...	... ...	... ...	... ...	...	...	...	S1
13106-0922	0.82 0.49	0.76	0.25 0.21	-0.31 -0.32	-0.34 -0.37	-0.87 -0.83	H	L	L	L:
13218+0552	0.85 0.49	0.83	0.31 0.27	-0.61 -0.61	-0.99 -1.01	-1.35 -1.30	...	...	...	S1
13305-1739	1.00 0.49	1.18	1.04 0.99	-0.47: -0.47:	-0.67: -0.71:	-1.14: -1.08:	S2	S2	S2	S2
13335-2612	0.96 0.49	1.09	0.31 0.26	-0.38 -0.38	-0.38 -0.41	-1.13 -1.07	H	L	L	L:
13342+3932	1.17 0.49	1.57	0.62 0.55	-0.28 -0.29	-1.22 -1.27	-1.77 -1.69	...	...	...	S1
13428+5608	1.02 0.49	1.22	0.57 0.51	0.01 0.00	-0.24 -0.27	-0.88 -0.82	S2	S2	S2	S2
13443+0802:NE	0.98 0.45	1.22	-0.33 -0.39	-0.22 -0.22	-0.42: -0.46:	-1.33 -1.26	H	H	H	H
13443+0802:SW	1.17 0.49	1.57	1.26 1.18	0.02 0.02	-0.21: -0.26:	-0.77 -0.69	S2	S2	S2	S2
13451+1232	1.04 0.49	1.26	0.96 0.90	-0.12 -0.13	-0.37 -0.41	-0.65 -0.58	S2	S2	S2	S2
13454-2956	1.16 0.49	1.54	0.76 0.68	0.02 0.01	-0.36 -0.41	-1.23 -1.15	S2	S2	S2	S2
13469+5833	1.03 0.45	1.34	-0.19 -0.25	-0.25: -0.25:	-0.44: -0.48:	-1.63: -1.56:	H	H	H	H

TABLE 5—*Continued*

Name IRAS FSC (1)	$\frac{H\alpha}{H\beta}$ log (2)	$E(B - V)$ (3)	$\frac{[O III]}{H\beta}$ log (4)	$\frac{[N II]}{H\alpha}$ log (5)	$\frac{[S II]}{H\alpha}$ log (6)	$\frac{[O I]}{H\alpha}$ log (7)	Spectral Type			
							[N II] (8)	[S II] (9)	[O I] (10)	Adopt (11)
13509+0442	0.97	1.20	-0.08	-0.36	-0.44:	-1.31	H	H	H	H
	0.45		-0.14	-0.36	-0.47:	-1.24				
13539+2920	1.13	1.56	0.07	-0.29	-0.40	-1.20	H	H	L	H:
	0.45		-0.01	-0.30	-0.45	-1.12				
14053-1958	0.63	0.31	0.60:	0.07:	-0.06:	-0.56:	S2	S2	S2	S2
	0.49		0.59:	0.07:	-0.07:	-0.54:				
14060+2919	0.84	0.90	-0.12	-0.34	-0.49	-1.42	H	H	H	H
	0.45		-0.17	-0.34	-0.51	-1.38				
14070+0525	1.39	2.08	0.67	-0.09	-0.14	-0.90	S2	S2	S2	S2
	0.49		0.57	-0.10	-0.20	-0.79				
14121-0126	1.12	1.45	0.22	0.05	-0.29	-0.89	L	L	L	L
	0.49		0.15	0.05	-0.34	-0.82				
14202+2615	0.80	0.79	-0.10	-0.34	-0.53	-1.39	H	H	H	H
	0.45		-0.14	-0.34	-0.55	-1.35				
14252-1550	1.20	1.64	0.22:	-0.25	-0.47	-1.20:	L	H	L	L:
	0.49		0.14:	-0.25	-0.52	-1.12:				
14348-1447:SW	0.99	1.15	0.17	-0.18	-0.23	-0.83	L	L	L	L
	0.49		0.11	-0.18	-0.27	-0.77				
14348-1447:NE	0.97	1.11	0.15	-0.18	-0.34	-0.98	L	L	L	L
	0.49		0.09	-0.19	-0.38	-0.92				
14394+5332	0.89	0.93	0.53	-0.03	-0.21	-0.71	S2	S2	S2	S2
	0.49		0.49	-0.03	-0.24	-0.66				
15001+1433	0.89	0.91	0.57	-0.19	-0.35	-1.21	S2	S2	S2	S2
	0.49		0.53	-0.19	-0.37	-1.16				
15043+5754	0.89	1.00	-0.02	-0.39	-0.47	-1.44	H	H	H	H
	0.45		-0.06	-0.40	-0.50	-1.39				
15130-1958	1.45	2.23	1.40	-0.08	-0.55	-1.13	S2	S2	S2	S2
	0.49		1.29	-0.09	-0.62	-1.01				
15206+3342	0.78	0.75	0.49	-0.65	-0.86	-1.60	H	H	H	H
	0.45		0.45	-0.65	-0.88	-1.56				
15225+2350	1.16	1.63	0.43	-0.32	-0.50	-1.27	H	H	L	H:
	0.45		0.35	-0.33	-0.55	-1.18				
15327+2340	0.95	1.05	0.06	0.38	0.02	-0.74	L	L	L	L
	0.49		0.01	0.38	-0.01	-0.68				
15462-0450	0.75	0.60	0.00	-0.42	-1.15	-1.84	...	...	...	S1
	0.49		-0.02	-0.42	-1.17	-1.81				
16090-0139	1.16	1.55	0.08	-0.11	-0.39	-1.11	L	H	L	L:
	0.49		0.01	-0.12	-0.44	-1.03				
16156+0146	0.79	0.69	0.97	-0.34	-0.46:	-0.83	S2	S2	S2	S2
	0.49		0.94	-0.35	-0.48:	-0.80				
16300+1558	0.92	1.00	0.09	-0.22	-0.29	-0.97	L	L	L	L
	0.49		0.04	-0.23	-0.32	-0.92				
16333+4630	0.91	0.96	0.20	-0.24	-0.38	-1.19	L	L	L	L
	0.49		0.16	-0.24	-0.41	-1.15				
16468+5200:W	0.92	0.99	-0.19	-0.19	-0.18	-1.69	L	L	H	L:
	0.49		-0.24	-0.20	-0.21	-1.64				

TABLE 5—*Continued*

Name IRAS FSC (1)	$\frac{H\alpha}{H\beta}$ log (2)	$E(B - V)$ (3)	$\frac{[O III]}{H\beta}$ log (4)	$\frac{[N II]}{H\alpha}$ log (5)	$\frac{[S II]}{H\alpha}$ log (6)	$\frac{[O I]}{H\alpha}$ log (7)	Spectral Type			
							[N II] (8)	[S II] (9)	[O I] (10)	Adopt (11)
16468+5200:E	1.07	1.33	0.06	-0.16	-0.09	-1.24	L	L	L	L
	0.49		-0.01	-0.17	-0.13	-1.18				
16474+3430	0.62	0.39	0.04	-0.32	-0.51	-1.25	H	H	L	H:
	0.45		0.03	-0.32	-0.52	-1.23				
16487+5447	0.70	0.48	0.20	-0.24	-0.44	-1.16	L	H	L	L:
	0.49		0.18	-0.24	-0.46	-1.14				
17028+5817:W	1.13	1.47	0.16	-0.25	-0.38	-0.97	L	H	L	L:
	0.49		0.09	-0.25	-0.42	-0.90				
17028+5817:E	0.76	0.70	0.05	-0.56	-0.51	-1.64	H	H	H	H
	0.45		0.01	-0.56	-0.53	-1.61				
17044+6720	0.87	0.86	0.43	-0.21	-0.44	-0.99	L	L	L	L
	0.49		0.39	-0.21	-0.46	-0.95				
17068+4027	1.10	1.48	0.33	-0.46	-0.44	-1.47	H	H	H	H
	0.45		0.26	-0.47	-0.48	-1.40				
17179+5444	1.01	1.19	1.01	0.12	-0.22	-0.93	S2	S2	S2	S2
	0.49		0.96	0.12	-0.25	-0.87				
20414-1651	0.98	1.21	-0.11	-0.27	-0.50	-0.97	H	H	L	H:
	0.45		-0.17	-0.27	-0.54	-0.90				
21208-0519:N	0.89	1.01	-0.10	-0.33	-0.54:	-1.42	H	H	H	H
	0.45		-0.15	-0.34	-0.58:	-1.37				
21208-0519:S	0.93	1.11	0.28	-0.37	-0.33:	-1.64	H	L	H	H:
	0.45		0.23	-0.38	-0.37:	-1.58				
21219-1757	...	...	-0.41	...	...	...	...	...	...	S1
	0.45		...	...	...	...				
21329-2346	0.78	0.67	0.00	-0.21	-0.35	-0.98	L	L	L	L
	0.49		-0.03	-0.22	-0.37	-0.95				
21477+0502	0.76	0.62	0.15	-0.24	-0.47:	-0.98	L	H	L	L:
	0.49		0.12	-0.25	-0.49:	-0.94				
22088-1813	0.69	0.54	-0.38	-0.32	-0.25:	-1.36:	H	L	H	H:
	0.45		-0.40	-0.32	-0.27:	-1.33:				
22206-2715	0.85	0.91	0.00	-0.31	-0.73	-1.11	H	H	L	H:
	0.45		-0.04	-0.32	-0.76	-1.06				
22491-1808	0.81	0.81	-0.15	-0.37	-0.60	-1.28	H	H	H	H
	0.45		-0.19	-0.37	-0.62	-1.24				
22541+0833:NW	0.62	0.29	0.12	-0.18	-0.39:	-1.44	L	L	H	L:
	0.49		0.11	-0.18	-0.40:	-1.42				
22541+0833:SE	1.63	2.62	0.98:	0.10:	-0.47:	...	S2	S2	...	S2:
	0.49		0.85:	0.09:	-0.55:	...				
23060+0513	1.06	1.33	0.95	-0.56	-0.72	-1.46:	S2	S2	S2	S2
	0.49		0.89	-0.57	-0.76	-1.39:				
23129+2548	1.10	1.40	0.12:	-0.19	-0.48	-1.09:	L	H	L	L:
	0.49		0.05:	-0.20	-0.52	-1.02:				
23233+2817	0.90	0.94	1.10	0.22	-0.46	-1.13	S2	S2	S2	S2
	0.49		1.06	0.22	-0.49	-1.09				
23234+0946	0.85	0.83	0.07	-0.09	-0.32	-0.96:	L	L	L	L
	0.49		0.03	-0.10	-0.34	-0.91:				

TABLE 5—*Continued*

Name IRAS FSC (1)	$\frac{H\alpha}{H\beta}$ log (2)	$E(B - V)$ (3)	$\frac{[O III]}{H\beta}$	$\frac{[N II]}{H\alpha}$	$\frac{[S II]}{H\alpha}$	$\frac{[O I]}{H\alpha}$	Spectral Type			
			log (4)	log (5)	log (6)	log (7)	$[N II]$ (8)	$[S II]$ (9)	$[O I]$ (10)	Adopt (11)
23327+2913	1.36	2.01	0.19:	-0.04	-0.40	-1.11:	L	H	L	L:
	0.49		0.09:	-0.05	-0.46	-1.01:				
23389+0300	0.96	1.09	0.65	0.33:	-0.08:	-0.11:	S2	S2	S2	S2
	0.49		0.60	0.32:	-0.11:	-0.05:				
23498+2423	0.87	0.87	1.04	-0.21	-0.52	-1.26:	S2	S2	S2	S2
	0.49		1.00	-0.21	-0.54	-1.22:				

Column (1) – Target name. († = non-photometric data)

Column (2) – Logarithm of  $H\alpha/H\beta$ .

Column (3) – Color excesses determined from the emission-line Balmer decrements.

Column (4) – Logarithm of observed and reddening-corrected  $[O III] \lambda 5007/H\beta$ .

Column (5) – Logarithm of observed and reddening-corrected  $[N II] \lambda 6583/H\alpha$ .

Column (6) – Logarithm of observed and reddening-corrected  $[S II] \lambda\lambda 6716, 6731/H\alpha$ .

Column (7) – Logarithm of observed and reddening-corrected  $[O I] \lambda 6300/H\alpha$ .

Columns (8) through (11) – Optical spectral types determined from the diagrams of Veilleux & Osterbrock (1987) involving  $[N II] \lambda 6583$  [column (8)],  $[S II] \lambda\lambda 6716, 6731$  [column (9)], and  $[O I] \lambda 6300$  [column (10)]. Column (11) lists the adopted spectral type. Meaning of the symbols: H = H II galaxies, L = LINER (‘low-ionization nuclear emission-line regions’), S2 = Seyfert 2 galaxies, and S1 = Seyfert 1 galaxies. A semi-colon (:) indicates galaxies with line ratios that do not correspond to the same spectral type in all three diagrams of Veilleux & Osterbrock (1987).

NOTE.— For each object, the emission line ratios listed on the first and second rows are normalized to the observed and dereddened fluxes of narrow  $H\alpha$  or  $H\beta$ , respectively. In Seyfert 1s, the ratios are normalized to the sum of the narrow and broad components of  $H\alpha$  or  $H\beta$ . These ratios are only listed for illustrative purposes since they cannot be used for spectral classification. The uncertainty on the emission line ratios is typically  $\pm 10\%$ . For entries with a colon (:) the uncertainty is approximately  $\pm 25\%$ .

TABLE 6  
SPECTRAL CLASSIFICATION AS A FUNCTION OF  $L_{\text{ir}}$

$\log \left( \frac{L_{\text{ir}}}{L_{\odot}} \right)$	<11 <sup>a</sup>	11–11.99 <sup>a</sup>	12–12.29	12.3–12.8
Number	29	68	77	31
H II region (%)	62	53	35	16
LINER (%)	31	32	41	35
Seyfert 2 (%)	7	13	21	23
Seyfert 1 (%)	0	2	3	26

<sup>a</sup>Data from luminous infrared galaxies in the BGS studied by VKSMS.